D0-note/PHYS-3493

August 1998

Definition of a Level 1 trigger using the Forward-Pre-Shower detector for the DØupgrade

Arnaud Lucotte and Mrinmoy Bhattacharjee

State University of New York, Stony Brook

Abstract

This document reviews the motivations and the expected performances of an electron and a photon trigger using the Forward Preshower (FPS) detector at level-1 for the DØupgrade.

In section 1 we recall the timing constraints resulting from the luminosities and bunch spacing configurations relevant for the run II. Section 2 describes the goal and concepts of an electron and photon trigger given the FPS detector design. Section 3 presents the current design of the FPS detector as well as a brief description of the readout scheme. Section 4 reports the performances of an electron trigger in terms of trigger efficiencies as well as pions background rejection. Section 5 is devoted to the results obtained for a photon trigger at L1. Eventually, occupancies and (single electron) trigger rates are estimated on dijet samples in Section 6. The dependence in the number of extra interactions (mbias interaction and underlying events) added to dijets events is described.

The last section details the characteristics of the data stream sent from the L1 Forward Preshower Front End to the L1 manager. The size (bits) as well as the flux of the trigger objects are regrouped here. A time estimation to form candidates with this algorithm is also presented, given the current scheme of the electronics readout system.

Contents

1 Introduction

At the run II, the instantaneous luminosity is expected to reach $\mathcal{L} = 2 \times 10^{32}\mathrm{cm}^2\mathrm{s}^{-1}$, with a bunch spacing of 132 ns. These new running configurations required a complete upgrade of the DØtrigger system.

The Level 1 (L1) trigger system has to operate at a rate of 7.6 MHz and a latency less than 4.2μs. The L1 trigger accept rate is fixed at 10 kHz, limited by tracking and calorimeter readout as well as deadtime minimization. Decision will be made upon the information coming from single detector systems, fed into a Trigger Framework [2].

The level 2 (L2) Trigger system is designed to make decision on a time scale of a few hundred μs. It consists of a global L2 processor (L2GLB) that operates on a list of objects coming from detector-specific pre-processors (L2PP). The L2 pre-processors are aimed at reducing the data flow sorted out from the front ends by providing a restricted list of objects. At this stage a factor 10 in rejection has to be achieved, leading to output rates of 1kHz. In the meantime, the amount of deadtime should not exceed 5% [1].

As for the FPS detector, the proposed L1 trigger is devoted to the detection of E.M. particles, identified as "electron-like" or "photon-like" candidates. It is based on the combination of a crude trigger signal coming from EM trigger towers in the End Calorimeter (EC) divided into quadrants, with a FPS signal within the same quadrant. Given the design of both the EC and the FPS detectors, the trigger logic will be contained locally to form FPS and EC candidates, wich are combined at the trigger manager level. The data stream is conditioned by the time interval between two bunches (132 ns) for the transfer of information from the Front End to the trigger manager; it is also constrained by the global time range of 4.2μs to form a list of objects sent from the L1 manager to the L2 trigger. These limitations thereby have implications on the type and flow of information that is used.

2 Conception of a electron/photon trigger with the FPS

2.1 Physics goals for a FPS trigger

The importance of the detection of electrons and photons in the forward region is described in [1]. We briefly recall below the major points of interest for the use of the FPS detector from the trigger point of view:

- Electrons from Top and W processes: improving the η coverage from 1.0 to 2.0 increases the geometric acceptance in the leptonic decays of the $t\bar{t}$ (with $t \to W$) and WW processes from 50 to 90%.

- Electrons from b-quarks: the FPS is the only device which may enable us to perform soft electron tagging in the forward region. Electron pairs originating from $b \to J/\Psi$ where $J/\Psi \to e^+e^-$ have very low P_T and a small opening angle. The End Calorimeter (EC) alone can not easily trigger on these events because of the high (QCD) background expected with low trigger thresholds (2 GeV in E_T). The combination of the FPS and the EC detector should allow us to reduce these numbers to acceptable rates.

- Electrons from SUSY particles: The production of gauginos may generate final states with 3 isolated electrons, as in the processes $\widetilde{W}_1\widetilde{Z}_2 \to eee$. These electrons typically have low P_T, so it is difficult to trigger on them with the End Calorimeter alone without facing huge QCD background trigger rates. As in the previous case, the use of the FPS detector should enhance the capability of triggering on multi-electron final state while reducing QCD background by an (several) order(s) of magnitude.

- Discrimination photons/electrons: In the topics described so far, it is important to discriminate electron from its background. One of these latter is composed with high energy photons close enough to charged hadron. It therefore appears relevant to ensure at an early stage that a good discrimination is achieved. The FPS detector should be a useful tool for this purpose, together with the End Calorimeter (EC), by providing hit locations before the showering processes occurs.

- Photons from $q\bar{q} \to W\gamma$ and $WW\gamma$: The detection of high energy photons may also be an important issue to measure the “radiation zero” effect as well as the trilinear coupling constants of a (effective) non-standard lagrangian. Again, the presence of a PreShower in the forward region may enhance tha capability to trigger on $e + \gamma$ final state.

In other words, the use of the FPS detector in the global trigger system, by improving the electron /pion discrimination, is expected to bring significant improvement with respect to a trigger based on the EM End Calorimeter towers alone. It should also help the trigger rates from QCD background around reasonable values for both level 1 and level 2.

2.2 Detection of electrons and photons with the FPS

The electron triggering is based on the measurement of large energy deposit in the layers behind the $2X_0$ thick converter, which is spatially matched with a hit consistent with a MIP in front. Rejection of photons from π^0 decays is obtained because they are not detected before the converter. The charged pions are eliminated because they tend not to shower and hence deposit little energy behind the lead.

The dominant background for electron signatures are photons from π^0 decays that convert before the FPS and charged hadrons that either shower early or overlap spatially with a photon. The presence of underlying events (resulting from the hadronization of spectator quarks) and of additional minimum bias interactions, constitutes a major concern to electron identification, specially with a large amount of material before the detector. Actually, a track that originates from the center of the detector traverses the beam pipe, the silicon vertex detector and sometimes the Central Fiber Tracking detector before reaching the FPS. This may cause photons to convert before the detector, thus mimicking the electron signature.

3 Particle ID using the FPS detector at Level-1

The identification of electrons and photons traversing the FPS detector is based extensively on the beam test results of four modules, performed during summer 97. Measured shower shapes and energy depositions in the four layers of the detector have been compared and used to tune the Monte Carlo simulation, based on the upgrade version of geant (version Feb 97 + upgrade FPS). Results are reported in detail in [5].

Because of time constraint during the Beam Test, electrons were targetted only in one region of the detector, around $\eta = 2.03$ (corresponding to an angle of $\theta \approx 15^o$). We generated our samples at the same angle to "calibrate" the MC simulations to the data, and then varied the angles of the generated particles to assess the η dependence of our results.

First we review the global design of the FPS that we used for the particle ID. We present then the criteria used to select electrons and photons.

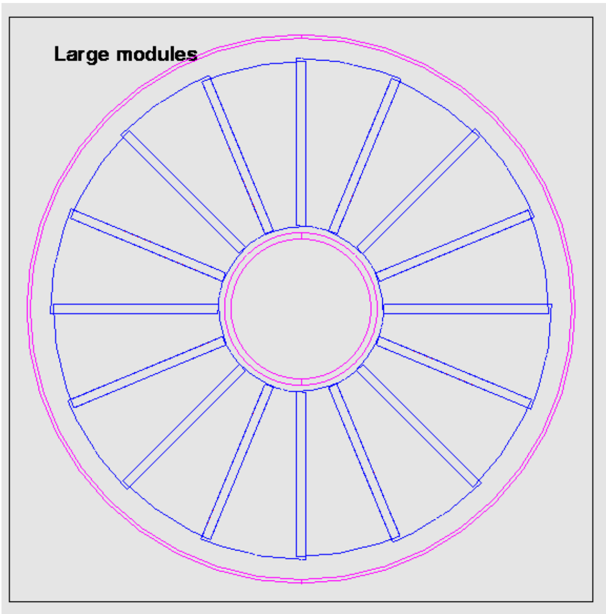

Figure 3.1: *Transverse view (X,Y) of the FPS detector. 16 modules of* 22.5^o *cover the azimuthal plane. Each of these modules define a "phi-sector" and is readout independently.*

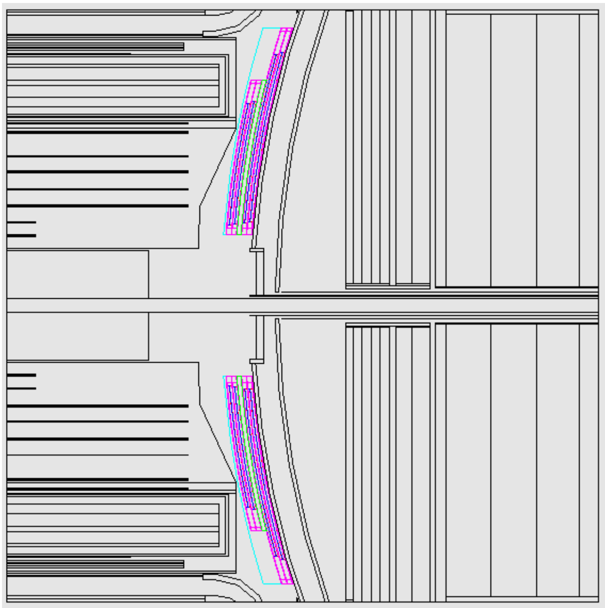

Figure 3.2: *Longitudinal view of the FPS detector. Each "phi-sector" is composed with two layers in front of a* $2X_0$ *lead sheet, and two layers behind. Each phi-sector is readout independently.*

3.1 Geometry and design of the FPS

The design of the FPS detector is detailed in [3]. The geometry of a half of the FPS is displayed in Fig. 3.1 (front view) and in 3.2 (transverse view). Briefly, the detector is composed of 4 layers and a $2X_o$ lead sheet converter. Two layers are located in front of the lead and are used to locate MIP depositions; two layers are behind the converter and are designed to measure showers generated by charged EM particles. Each of these layers is made of 16 modules covering a "phi-sector" of 22.5°. A module is composed of 7.8 mm-wide and 6.0 mm-high triangular strips traversed by a scintillating fiber. Strips are orientated differently depending on the layer index: in layers 1 and 3 strips are orthogonal to the right edge of a module (v- strips); in layer 2 and 4, they point in the opposite direction and are perpendicular to the left edge (u- strip), so that a stereo angle of 22.5° is formed between the two types.

A "phi-sector" (22.5°) is thus composed of a superposition of two front layers, as well as of two rear layers with respect to the lead. In the following we designate the first ones (front) as "upstream" or "MIP" layers, whereas the latter (rear) are named "downstream" or "shower" layers. "Phi-sectors" are read out independently of each other. Note that there is an 1-inch wide region where two adjacent modules overlap.

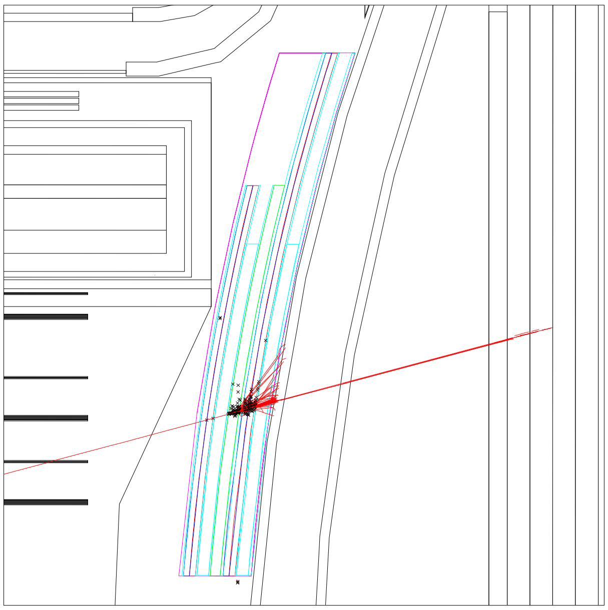

Figure 3.3: *50 GeV electron traversing the four layers of the FPS detector.*

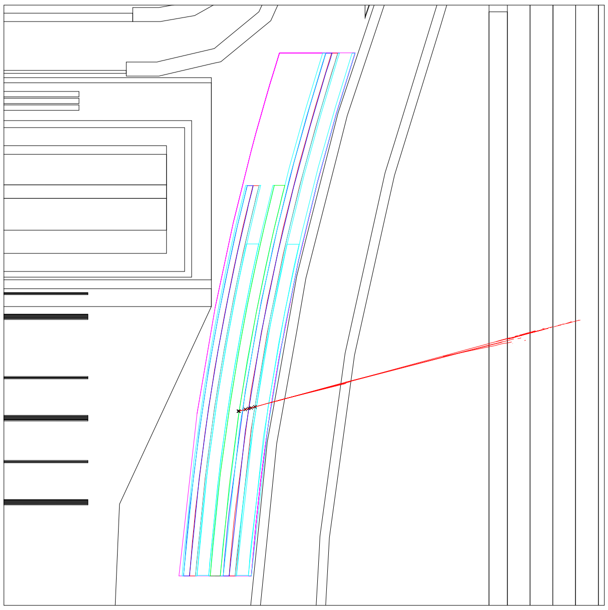

Figure 3.4: *50 GeV photon traversing the 4 layers of the FPS detector.*

Fig. 3.3 and 3.4 respectively display typical 50 GeV electron and photon traversing the FPS detector. Their characteristics are now described in the following sections. Regarding the electron ID, we put emphasis on pion rejection. As for the photon ID, we insisted on the electron/photon discrimination.

3.2 Particle identification: electron

At Level-1, the FPS detector is intended to identify objects which are either "electron like" or "photon like". The algorithm of identification is based on the energy depositions as seen in the four layers of the FPS detector. Both Monte Carlo and results from the Beam test of two FPS modules are used in this first sub-section to justify selection cuts. In the following we use a MIP as the energy unit. For these studies, we define 1 MIP = 1 MeV.

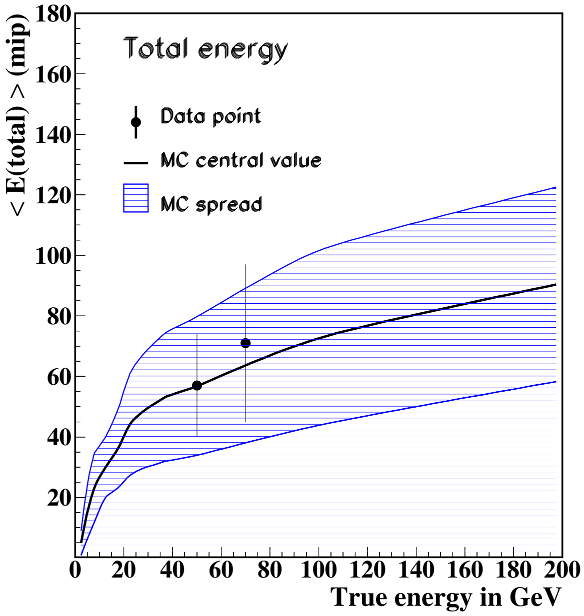

Figure 3.5: *Total energy deposited by an electron in one of the shower layers. Dots are data.*

3.2.1 Shower layers

Fig. 3.5 displays the total energy deposited in the shower layers as a function of the energy of the electron. The two points come from measurements performed during the FPS test beam [5], whereas the curves are computed from simulated events. There is no one-to-one correlation between the particle's energy and the amount of charge spawned by the traversing particle: the correlation weakens as electrons reach higher energy values. As a consequence, we do not expect to improve selection efficiency by using the full information from the shower energy. On the other hand, a selection based on a high threshold in the central strip alone appears to be quite efficient, since electrons tend to deposit about 35% of the total energy measured in the FPS detector in the central strip, as seen in Fig. 3.7 and 3.8. This result is independent of the (true) energy of the electron. As a consequence, the detection of electrons will be essentially based on the choice of a high threshold in the layers behind the converter.

Monte Carlo electron and pion samples generated between $2.5 \leq P_T \leq 35$GeV have been used to set the high threshold. Fig. 3.6 shows the dependence of the efficiency on the downstream threshold. The necessity of triggering low P_T electron leads us to keep the threshold as low as 5 MIPs. Pion rejection as well as (QCD) trigger rates will be considered in the following.

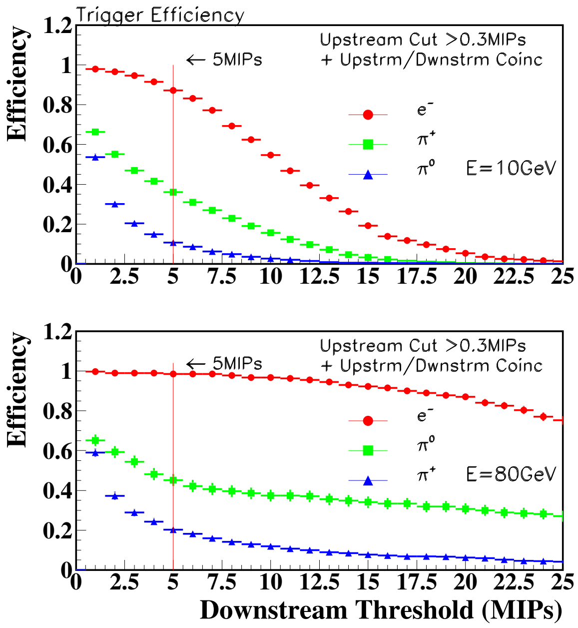

Figure 3.6: *Dependence of the electron and pion selection efficiency on the high threshold (shower layers). The low threshold is set at 0.3 MIPs (in MIP layer), also required is a spatial coincidence between shower and MIP layer.*

Another issue in the shower layer is the relevance of an isolation cut. Shower shapes for 10 GeV and 60 GeV electrons/pions are compared in Fig. 3.7 and 3.8 where the best “region” (chosen to optimize pion rejection) to apply isolation criteria is defined. The size and the location of the isolation window to look at depend strongly on the particle energy: in the lower energy range, the best window is far away from the center of the shower (strips 7 to 10), whereas for higher values, a relevant window is provided by more central strips (4-5).
However, in a realistic environment, the presence of underlying events and minimum bias interactions tend to reduce the effectiveness of such criteria. Fig. 3.9 and 3.10 show the efficiency of isolation cuts versus the effects on the pion contamination. A slight increase of a few percent is measured with respect to an algorithm where no isolation condition is required. This result certainly does not justify the use of an isolation cut in the shower layers at the trigger level.

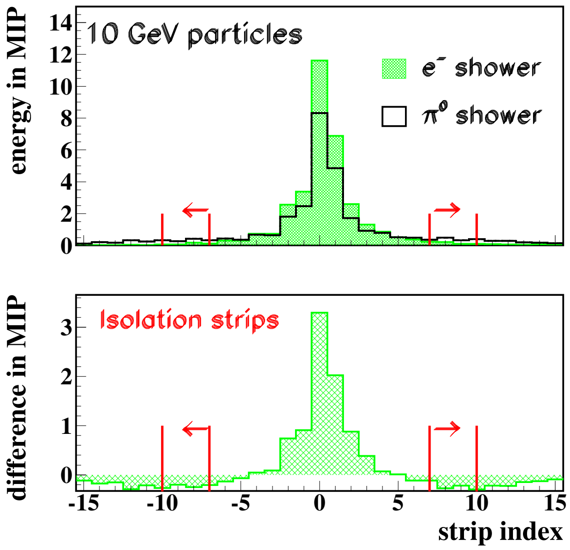

Figure 3.7: *Energy shower for 10 GeV electron and neutral pions (top). Difference in energy/bin (bottom)*

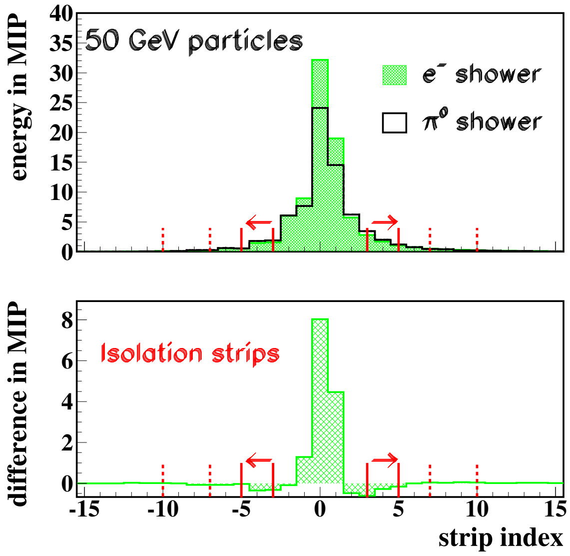

Figure 3.8: *Energy shower for 60 GeV electron and neutral pions (top). Difference in energy/bin (bottom)*

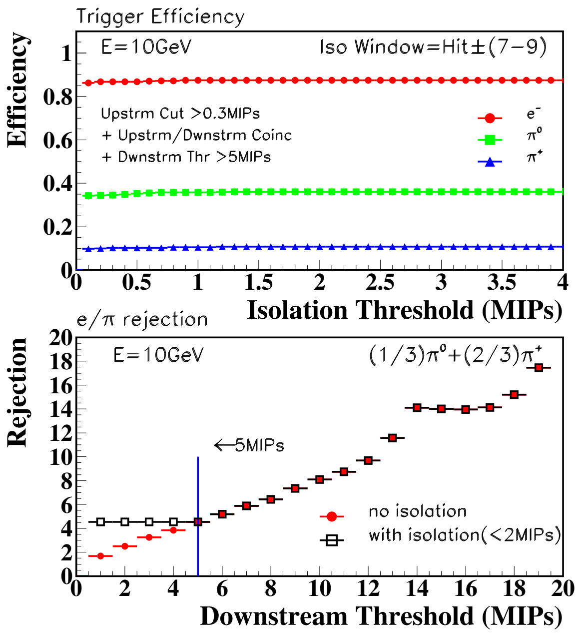

Figure 3.9: *Efficiency of the isolation cut and effects on pions rejection at 10 GeV.*

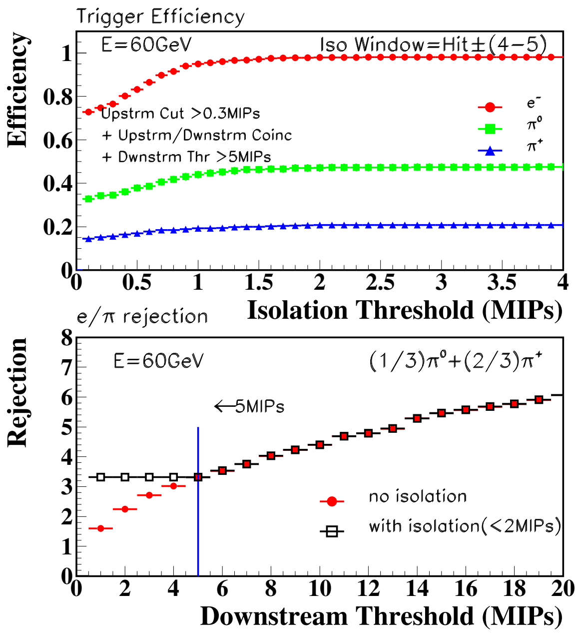

Figure 3.10: *Efficiency of the isolation cut and effects on pions rejection at 60 GeV.*

3.2.2 MIP layers

Regarding upstream layers, electrons are expected to deposit a fraction of a MIP in two adjacent strips, whereas π^0 are not expected to leave any hit in the layer. However, due to the presence of material in front of the FPS detector (SVX and 4-layers CFT), e^+e^- from pions and photons are expected to strike strips in front of the lead. We counted from Monte Carlo the number of π^0 converted before reaching the FPS layers by switching ON/OFF the GEANT simulation of inner trackers: around 30% of the π^0's leave a signal in the MIP layers as a result of conversions.

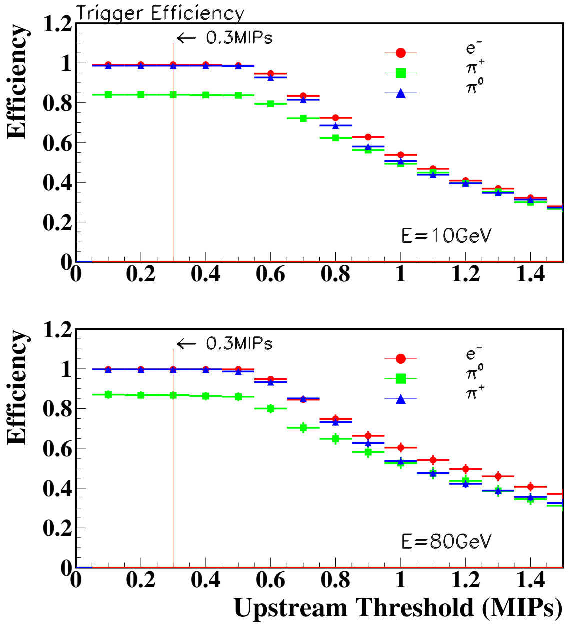

Figure 3.11: *Dependence of the electron and pions selection efficiency in the low threshold (in MIP layers). No threshold is applied in the shower layers.*

To select electrons, we chose to require that one strip measure at least 0.3 MIP as a confirmation of a larger deposition downstream. The value chosen for this threshold is set by constraints coming both from electron selection efficiency and pion rejection. The efficiency dependence in this requirement is presented in Fig. 3.11.

We also defined a coincidence window between the location of hits downstream and MIP depositions upstream. As we do not have the time to reconstruct (η, ϕ) at L1, the coincidence is defined between MIP and shower for the u- and the v- layers separately using the strip index. Two parameters have to be set: the offset between the upstream MIP location and the strip struck downstream; the width of the window in which we want to check for the presence of a confirmation MIP signal. These two parameters obviously depend on the η of the particles and so we produced two electron samples at $\eta = 2.33$ (lower edge) and at $\eta = 1.59$ (higher part of module).

Fig. 3.12 shows the variation of the selection efficiency with the value taken for the offset.

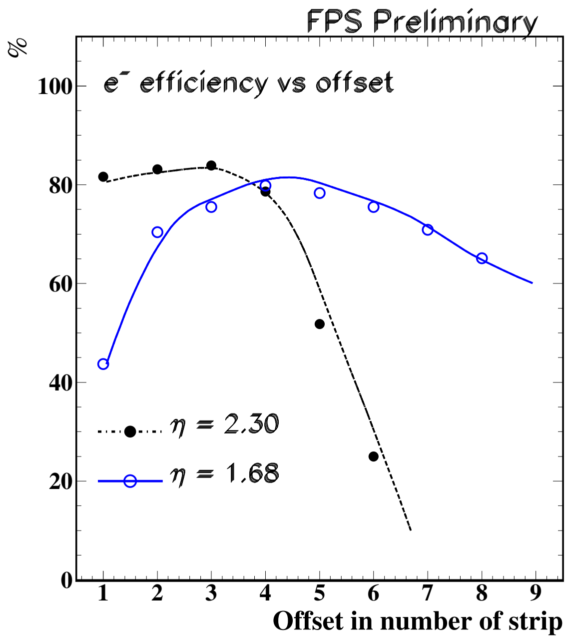

Figure 3.12: *Selection efficiency as function of the offset between the downstream deposition and the coincident MIP signal upstream. Shower and MIP thresholds are set (resp.) at 5 MIPs and 0.3 MIPs.*

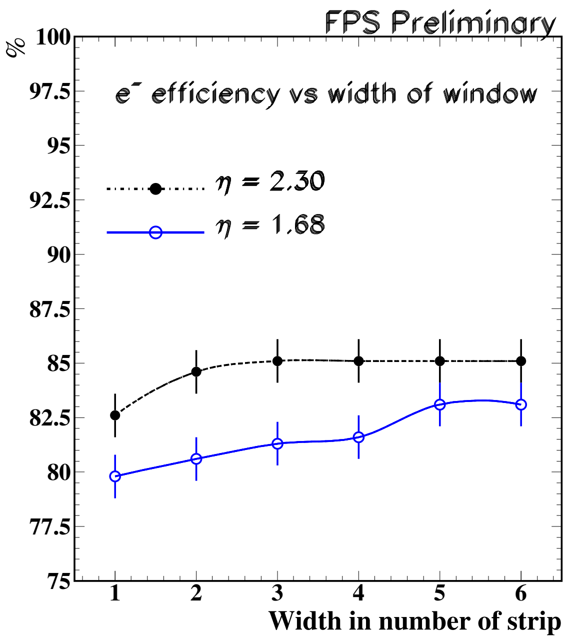

Figure 3.13: *Selection efficiency as function of the width of the coincidence window between the shower and the MIP signal upstream.Shower and MIP thresholds are set (resp.) at 5 MIPs and 0.3 MIPs.*

The maximum efficiency is found for an offset of 3 in the first case (electron close to the lower edge), while a 4-strips offset maximizes the efficicency for electron higher in the module.

Fig. 3.13 displays the variation of the efficiency as function of the size of the upstream window. A $\pm$3-strips wide window turns out to keep a high efficiency for all samples, whatever the choice for the offset may be between 3 and 6.

To account for the η dependence of the particle in the FPS, we decided to set a fixed value for the off-set, whatever the shower location may be behind the lead, and to widen the window in which the MIP deposition is looked for: this combination helps us to keep a high selection efficiency for electrons in the whole FPS acceptance while simplifying the logic in the L1 electronics by limiting the number of operations per downtream hit. Thus, for each shower deposition in strip $\mathrm{I}_{\mathrm{shower}}$, we require that a MIP be seen in strip $\mathrm{I}_{\mathrm{mip}}$ such that:

$$\mathrm{I}_{\mathrm{mip}} \in (\mathrm{I}_{\mathrm{shower}} - 4) \pm 3 \text{ strips}$$

The use of an isolation criteria upstream has also been investigated. Because of the presence of minimum bias interactions, no significant improvement has been observed in the (neutral) pion and photon rejection.

3.3 Particle identification: photon

The design of a L1 photon trigger algorithm is motivated by the fact that, in absence of any upstream material, the photon does not leave any signal in the MIP layers, but, it showers in the $2X_0$ thick lead absorver and deposits large energy in the Shower layers, Fig. 3.4. However, in the not so ideal environment of the upgraded detector, before hitting the FPS, the photon has to traverse through the beam pipe, the SVT & sometimes the CFT, where it might convert into e^+e^- pairs. Also, the presence of the additional interactions make its identification even harder.

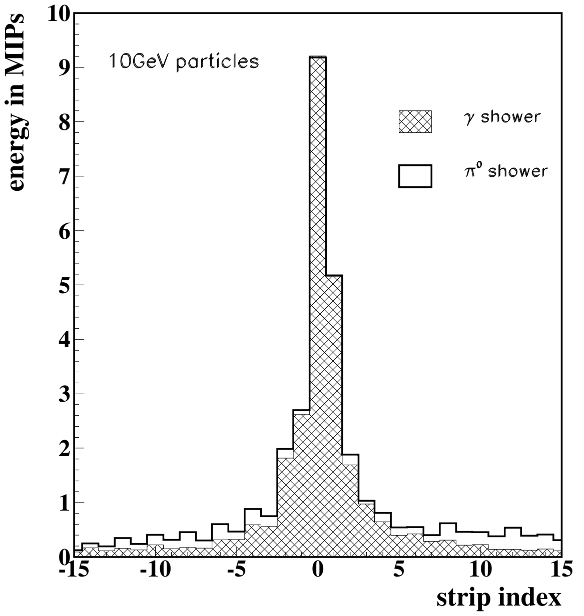

Figure 3.14: *Photon and neutral pion shower profile in the FPS (***10GeV***).*

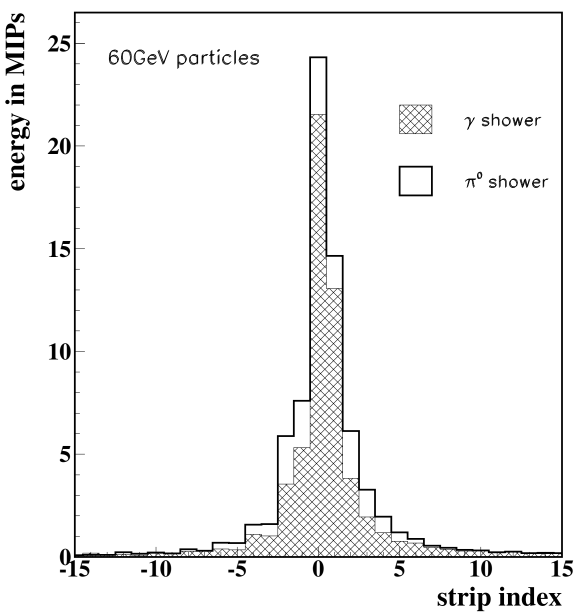

Figure 3.15: *Photon and neutral pion shower profile in the FPS (***60GeV***).*

The photon trigger is intended to provide the necessary discrimination between these "electron like" and "photon like" objects. On the other hand, the π^o's and γ's behave very simillarly in the FPS detector, Fig. 3.14 and 3.15. At low energies (10GeV), there is no difference in the peaks of these showers & even in the wings of the showers, the difference amounts to a maximum of 0.3MIPs. For higher energies (60GeV), the π^o shower peak becomes significantly larger. But, due to the similar behaviour of these particles in the MIP layers, discrimination becomes almost impossible. As a result, at L1, the FPS is not expected to give good discrimination between π^o's and γ's. It will require some amount of sophisticated shape analysis, which is not possible at L1.

The presence of a high energy hit in the shower layers (both u- & v-) with a veto in the appropriate region of the MIP layers is expected to signal a photon hitting the FPS detector.

In what follows, a L1 photon trigger is developed and tuned by studying its dependence on various parameters.

3.3.1 Shower layers

In this section, the dependence of the photon algorithm on a threshold in the shower layers will be studied. In the previous section the necessity of a high threshold for the signal in the shower layers was demonstrated. Figs. 3.16 and 3.17 show the dependence of photon selection efficiency on downstream threshold for photon energies of 10GeV & 80GeV. These efficiencies were caculated with a veto window of -4$\pm$3 and a veto threshold of $<$0.3MIPs. Also shown are selection efficiencies of electrons for this algorithm. For both photons and electrons the efficiency goes down with increasing downstream threshold. The bottom plots show the γ/e^- rejection as a function of the downstream threshold. As can be seen from the plots, at a downstream threshold of 5 MIPs, the rejection remains between 5-3.5 (low - high energy). Above this value, although the rejection rises the photon selection efficiency becomes too low for the trigger to be useful. Also, the 5 MIPs threshold fits in nicely with threshold proposed for the L1 electron trigger. Hence, to select photons using the FPS, we require that there should be at least one strip with a energy deposition more than 5MIPs in both the layers behind the lead converter.

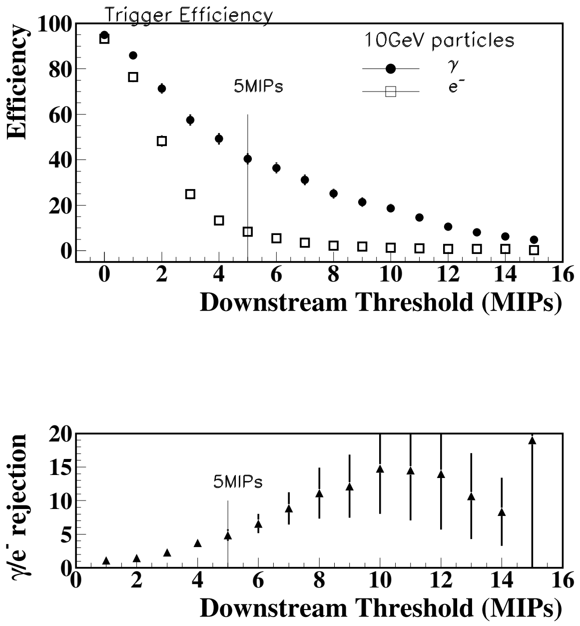

Figure 3.16: *Trigger efficiency as a function of downstream threshold. The upstream VETO<0.3MIPs (***10GeV***).*

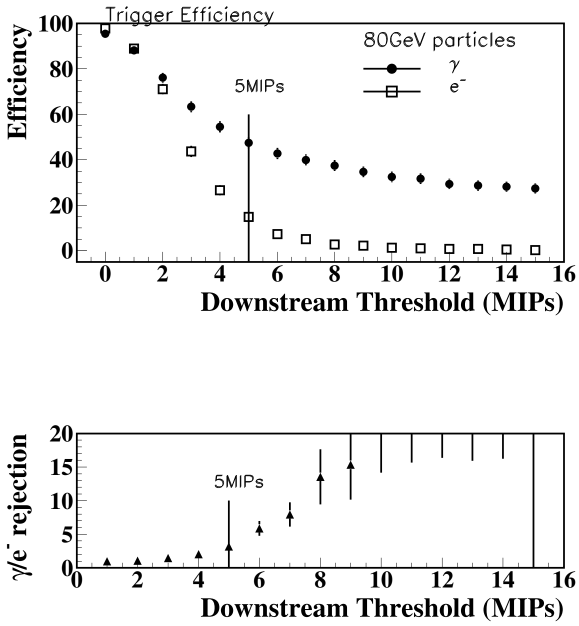

Figure 3.17: *Trigger efficiency as a function of downstream threshold. The upstream VETO<0.3MIPs (***80GeV***).*

3.3.2 MIP layer VETO

Figs. 3.18 and 3.19 show the dependence of photon selection efficiency on a upstream veto threshold for 10GeV and 60GeV particles. For any strip, I_s, above a certain threshold in a shower layer, all the $\mathrm{I_s} - 4 \pm 3$ strips in the corresponding MIP layer were required to be below a veto threshold. If this condition is satisfied for both the u & v MIP layers then a photon is triggered. In both the plots, the upper curves show the selection efficiency of photons and electrons as a function of the veto threshold when no thresholds were required for the shower layers (>0MIPs). No discrimination between photons and electrons can be seen from these curves. The lower plots show the same, but when a threshold of >5MIPs is required for the signal in shower layers. This gives a rejection factor of roughly 5-3.5 from low to high energy. This demonstrates the requirement of a high threshold in the shower layers to discriminate between photons and electrons.

The width of the veto window was varied in order to study its effect on the selection efficiency. While, the reduction of this window width does not have a significant effect on the efficiency, its increase from ±3 to ±5 and ±7 decreases the photon efficiency somewhat. The optimal value for the veto window width was found to be ±3 strips.

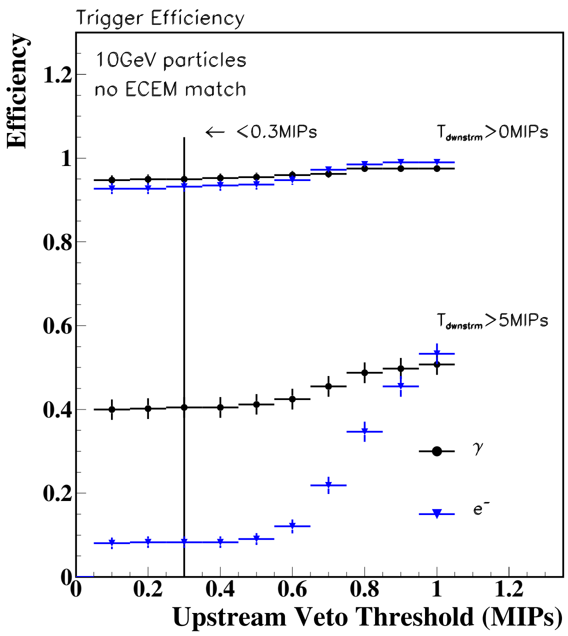

Figure 3.18: *Trigger efficiency as a function of upstream VETO threshold (***10GeV***).*

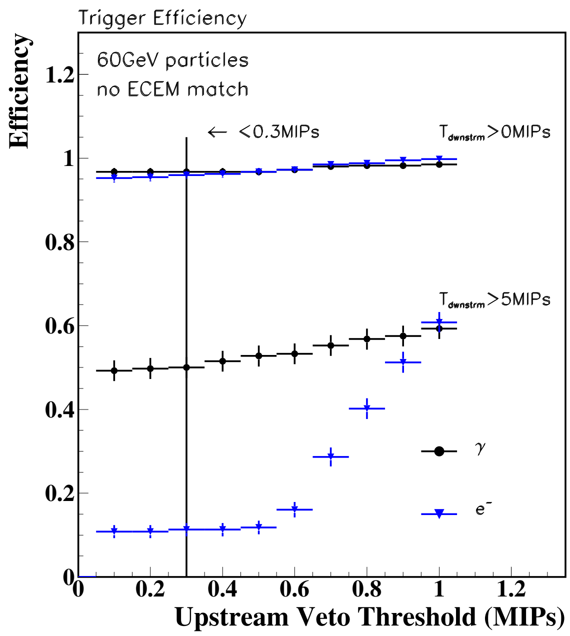

Figure 3.19: *Trigger efficiency as a function of upstream VETO threshold (***60GeV***).*

From Figs. 3.18 and 3.19, the efficiency and rejection remains stable up-to a veto threshold of 0.3MIPs, above which, as the electron deposits a fraction of a MIP in the hit strips in the MIP layers, the electron efficiency begins to rise at a faster rate than that of the photons. This washes away the rejection power. Hence, to select photons, we choose that all strips within -4$\pm$3 of the strip passing a high threshold in the shower layer to have energy less than 0.3MIPs.

4 Level-1 electron and photon trigger

Trigger efficiencies have been computed on ISAJET generated events fully reconstructed through the upgrade version of GEANT (Feb-97– All detectors but FPS + Feb-98 FPS). In these samples, single particles ($e^-, \gamma,\ \pi^0,\ \pi^\pm$) have been targetted around $\eta = 2.03$ and $\phi = 101.25^0$, which corresponds to the center of the 5^{th} FPS sectors. All samples have then been overlaid with two additional minimum-bias interactions, modelled with low $\mathrm{P_T}$ dijet events produced with ISAJET.

In the first sub-sections, we report on the trigger efficiencies computed only with the information coming from the FPS detector. However, in a realistic environment, the triggering of electron or photon candidates is based on the coincidence of a FPS signal with one from the End Calorimeter (EC). Because of timing constraint at L1, only a sum of signals from the EM towers is available, over a quadrant, hafl or full azimuth. Several options have been considered for the combination of these two signals. They will be described in the trigger rates section. In the following, we require two coincident signals (from FPS and EC) within the same quadrant. Thus, the interesting trigger objects are:

E.M. object	EM =	FPS downstream .AND. EC Quad
e object ($5 \leq$ strip ≤ 105)	ELE =	FPS upstream .AND.EM
γ object ($5 \leq$ strip ≤ 105)	GAM =	EM .AND..NOT. ELE
e^- object (strip ≤ 5 .or.$105 \leq$ strip)	ELE =	EM

where FPS downstream and FPS upstream are defined as:

- FPS downstream: energy deposition above $\mathrm{T_{down}} = 5$ MIPs must be measured in a single strip in both u and v layers behind the lead converter.
- FPS upstream: at least one hit must be seen in both u and v layers in front of the converter, with an energy above $\mathrm{T_{up}} = 0.3$ MIP. This signal must be located within a 3-strips wide window, centered on the strip corresponding to the centre of the shower shifted by 4 strips.

The definition above is valid up to the region for which index = 105 (in strip number), since in the outer part of the detector there is no corresponding MIP layer in front. A similar effect is expected in the lower edge of the module, near the beam pipe, where the 5 first strips in the shower modules do not have any counterpart upstream. By convention we chose to label these signals as ELE candidates, as we can only detect the shower energy and hence identify the particle as “electron like”.

4.1 The electron trigger: ELE trigger

Selection efficiencies resulting from the requirements presented above are reported in table 1 for electrons generated with transverse momentum ranging from 2.5 to 35.0 GeV/c. A complete comparison with pion selection is displayed in Fig. 4.20, 4.21, 4.22 and 4.23.

4.1.1 Performance of the ELE trigger

When no coincidence with the EC is required (see column 2), results show that the electron efficiencies are above 87% for $P_T = 2.5$ GeV/c and 95% for higher P_T particles.

E/P_T in GeV	No EC threshold	EM tower threshold (EC)		
		$E_T \geq 2$ GeV	$E_T \geq 5$ GeV	$E_T \geq 10$ GeV
10 / 2.5	87.6±0.9%	86.5±2.3%	—	—
20 / 5.0	95.1±0.6%	96.6±0.8%	61.1±3.1%	—
40 /10.0	97.8±0.4%	98.9±0.4%	99.1±0.4%	100.0±0.0%
60 / 15.0	98.6±0.3%	99.3±0.4%	99.6±0.3%	99.7±0.3%
80 / 20.0	98.9±0.5%	99.4±0.6%	99.4±0.6%	99.1±0.6%
130/ 35.0	98.2±0.7%	98.9±0.8%	98.9±0.8%	98.9±0.8%

Table 1: *Selection efficiency estimated on samples of single electron + 2mbias interactions. FPS Thresholds have been set at 0.3 MIPs upstream and 5 MIPs downstream. In column 2, only the FPS detector is used. Columns 2,3 and 4 show efficiencies of electrons already triggered by (at least) one EM tower in the EC quadrant with threshold of 2, 5 or 10 GeV in* E_T.

Columns 3,4 and 5 of Table 1 report the efficiency with which an event, already triggered by at least one E.M. tower in the End Calorimeter, is also seen in the FPS detector. As mentioned earlier, an electron is selected when the signal from the FPS is in coincidence with a EM trigger tower located in the same quadrant.

From this table, electrons above $P_T \geq 10$GeV are selected with more than 99% efficiency relative to the EC triggering. This result is relevant for W/Z electrons which typically are selected with more than 10 GeV in E_T. For low $E_T \geq 2$ GeV threshold, electrons are selected with a good efficiency. However, the trigger rates in this range may be prohibitive. They will be presented in the trigger rates section. All these results are also regrouped in Fig. 4.22 as a function of the electron P_T.

The above selection is based on the information coming from one (at least) E.M. tower located within the same quadrant of the FPS signal. We enlarged this test asking for a "cruder" coincidence with one 1/2 of the EC, and one with the entire EC. Results show that electron trigger efficiency is stable as we vary this requirement. The impacts of these changes are relevant with respect to the trigger rates. They are detailled in section 6.

Pion efficiencies have been computed for pion samples $\left(\frac{1}{3}\pi^0 + \frac{2}{3}\pi^-\right)$ and are reported in table 2. Column 2 presents the results when the FPS alone used for triggering. Columns 3,4 and 5 again report the selection efficiency relative to the EC triggering as defined previously for the electrons.

E/P_T in GeV	No EC threshold	EM tower threshold (EC)		
		$E_T \geq 2$ GeV	$E_T \geq 5$ GeV	$E_T \geq 10$ GeV
10 / 2.5	23.7±1.5%	10.5±7.0%	—	—
20 / 5.0	26.9±1.6%	38.0±3.5%	—	—
40 / 5.0	31.8±1.6%	42.3±3.9%	49.9±5.8%	—
60 / 15.0	32.6±1.7%	44.8±2.8%	39.7±2.9%	30.6±6.3%
80 / 20.0	32.3±1.9%	46.1±4.5%	45.9±4.7%	50.0±6.2%
130/ 35.0	34.6±1.7%	45.7±2.8%	50.8±2.8%	51.9±3.0%

Table 2: *Selection efficiency estimated on samples of single pions + 2mbias interactions. FPS Thresholds have been set at 0.3 MIPs upstream and 5 MIPs downstream. In column 2, only the FPS detector is used. In columns 2,3 and 4 efficiencies concern electrons already triggered by (at least) one EM tower in the EC quadrant with threshold of 2, 5 or 10 GeV in* E_T.

For a trigger based on the FPS detector alone, the comparison pion vs electron is presented in Fig. 4.20, which displays the trigger efficiency as function of P_T for both electron and pion. The ratio electron / pion, which is a good indication of the background rejection to isolated electrons, is displayed in Fig. 4.21. At each point, this ratio is computed by using the electron selection efficiency divided by the pion efficiency, where we take for pions the weighted sum $\left(\frac{1}{3}\pi^0 + \frac{2}{3}\pi^-\right)$. A global ratio eletron/pion above 3 is observed if the FPS detector alone is used.

For a trigger combining EC quadrant with the FPS detector, the ratio electron / pions is displayed in Fig. 4.23 as a function of the P_T of the particles for E.M.thresholds of 2 , 5 and 10 GeV. Rejection rates are found around 2-2.5 if a threshold of $E_T = 2.0$ GeV is applied. This ratio, which is relevant for J/Ψ selection, must be improved at the level 2.
For higher EM tower thresholds, which corresponds to W- or Z-physics, rejection rates are quite steady with the P_T of the particles, while a change from 10 to 5 GeV in the threshold does not affect the results significantly: in both cases, a rejection around 2 is observed. Of course, the setting of this EC threshold affects significantly the global trigger rates on QCD background. This question is presented in section 6.

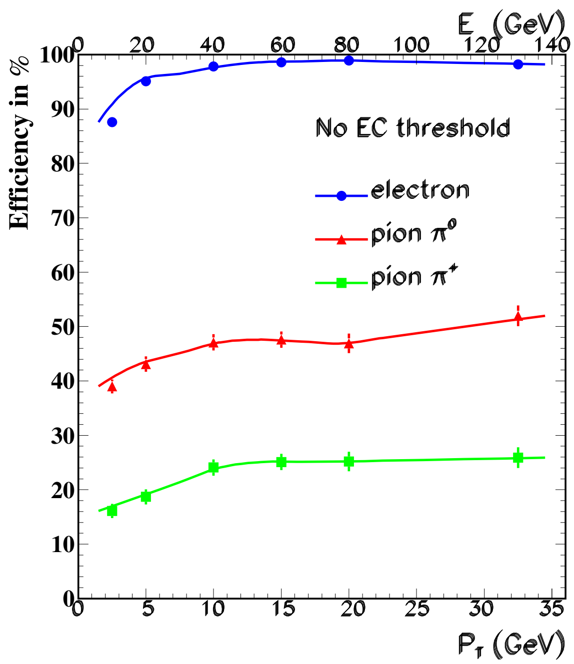

Figure 4.20: *Electron and pions efficiency as function of the transverse momenta of the particles. Requirements are:* $T_{up} = 0.3$MIP and $T_{down} = 5$ MIPs.

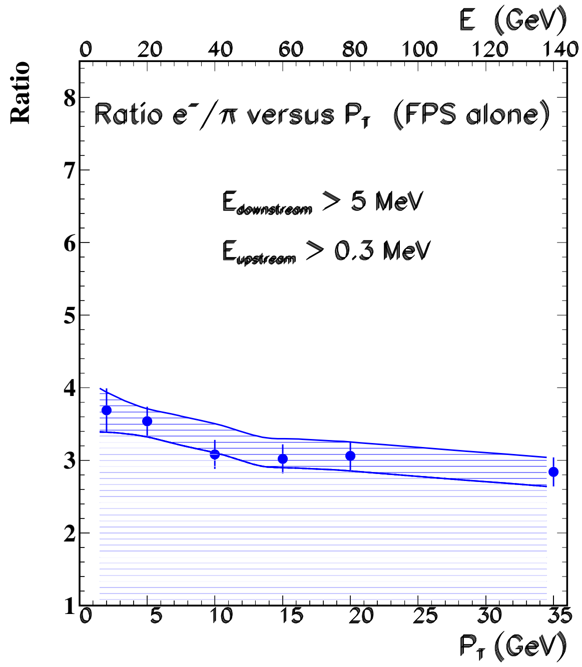

Figure 4.21: *Electron / pion ratio as function of the transverse momenta of the particles. Requirements are:* $T_{up} = 0.3$MIP and $T_{down} = 5$ MIPs

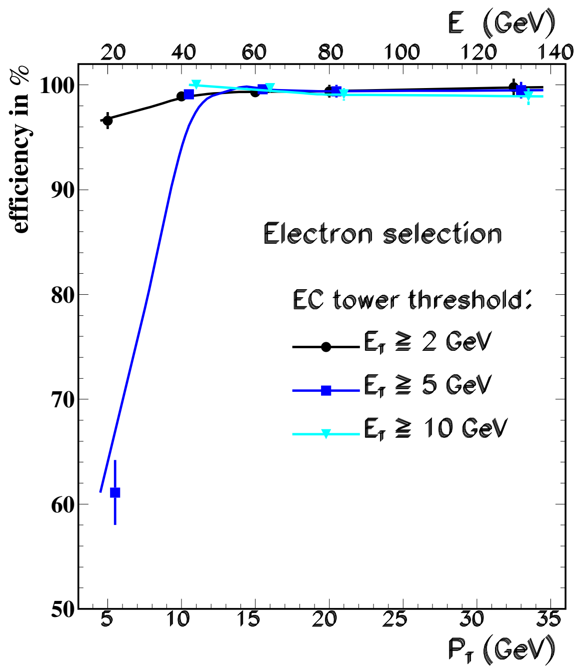

Figure 4.22: *Electron selection efficiency as function of the transverse momentum, for electrons already triggered by the EC. The effects of three EM tresholds are shown.*

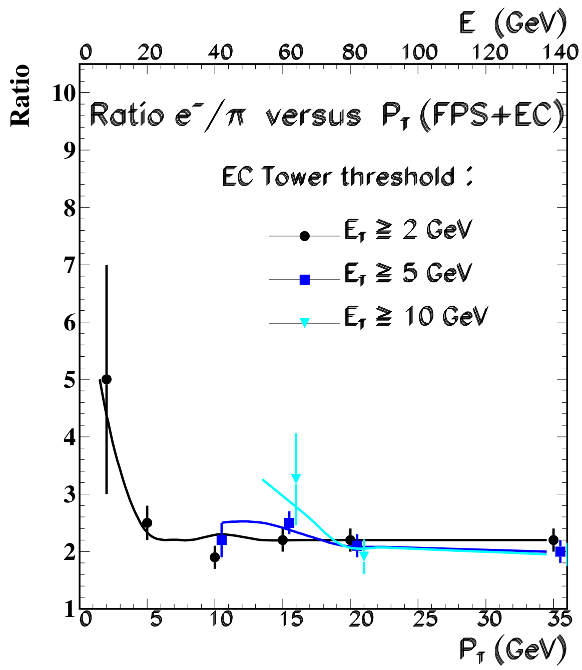

Figure 4.23: *Electron / pion ratio as function of the transverse momentum of particles already triggered in the EC. The effects of three EM tresholds are shown.*

4.1.2 Dependence in η of the ELE trigger

The L1 algorithm depends on the location of the energy deposition in the shower layers. It is thus necessary the study to stability of the trigger efficiency for different hit location. To the electron samples used in the previous sections, we added new samples generated at E = 60 GeV at three fixed pseudo-rapidity values: around $\eta = 1.59$ (upper edge of downstream modules - no upstream coverage), around $\eta = 1.65$ (upper edge of small modules) and finally around $\eta = 2.50$ (lower edge of modules).

Fig. 4.24 reports the efficiencies as measured for the four samples as function of η. Significant effects are observed for particles generated in the lower part of the module, where a loss of about 20% is measured in the selection efficiency.

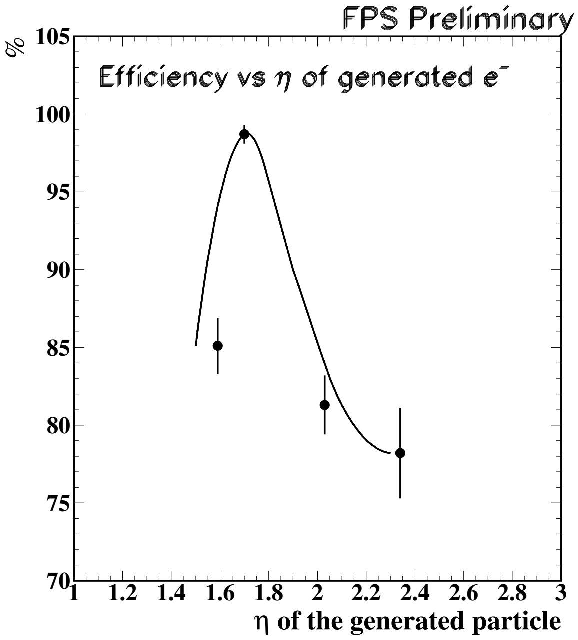

Figure 4.24: *Efficiency for 60 GeV electrons as function of η of the generated particle. The physical limits of the FPS detector in η are respectively 1.5 (high edge of large module) and 2.5 (low edge of a module).*

This variation comes mainly from the spread with which particles are reconstructed around the initial (generated) direction. This causes some of them to be outside the FPS acceptance, especially for particle generated in the very high eta region where a 20% effect is seen. This statement is valid for both electron and photons, which are affected the same way. Therefore no change in the rejection factor is expected in these extreme regions.

4.2 The photon trigger: GAM trigger

Photon trigger efficiencies have been calculated using the algorithm defined above. The only difference from the electron algorithm is that a veto is applied in the window in front of the lead instead of a MIP deposit requirement.

4.2.1 Performance of the GAM trigger with the FPS alone

Table A, lists the efficiencies of this trigger in different P_T ranges. Figs. 4.25 and 4.26 shows the efficiency of this trigger for photons as well as electron rejection (1-efficiency), respectively. Efficiencies are found to be $\geq 40\%$ for $P_T \approx 2.5$GeV and $\geq 54\%$ for $P_T \approx 32.5$GeV.

$\mathrm{E/P_T}$ in GeV	No EC threshold	EM tower threshold (EC)		
		$E_T \geq 2$ GeV	$E_T \geq 5$ GeV	$E_T \geq 10$ GeV
10 / 2.5	40.5±2.5%	22.7±8.9%	—	—
20 / 5.0	48.2±2.5%	47.1±2.7%	—	—
40 /10.0	47.2±2.5%	47.2±2.5%	42.5±3.1%	—
60 / 15.0	50.0±2.5%	50.0±2.5%	48.7±2.5%	45.3±4.6%
80 / 20.0	47.5±2.5%	47.5±2.5%	47.5±2.5%	45.6±2.9%
130/ 35.0	54.8±2.5%	54.8±2.5%	54.8±2.5%	54.6±2.5%

Table 3: *Selection efficiency estimated on samples of single photon + 2mbias interactions. VETO threshold of $\leq$0.3 MIPs upstream and 5 MIPs downstream are appliedxauto-fill-mode. In column 2, only the FPS detector is used. Columns 2,3 and 4 show efficiencies of electrons already triggered by (at least) one EM tower in the EC quadrant with threshold of 2, 5 or 10 GeV in* $\mathrm{E_T}$.

4.2.2 Performances of the GAM trigger with EC + FPS

Table A, reports the efficiencies of photon selection when along with the requirements in the FPS, an additional requirement on the backing End Cap EM calorimeter quadrant is also asked. The requirement on the calorimeter is that at least one tower in the quadrant behind the FPS module hit by the particles is above a certain threshold. The results reported in this table are for thresholds of 5 and 10GeV. These results are shown in Fig. 4.27. A 5GeV threshold on the ECEM quadrant does not have any significant effect on photon selection, however, a threshold of 10GeV reduces the efficiency almost by half. Fig. 4.28, shows the dependence of photon to electron rejection factor on the ECEM tower threshold in a quadrant. The rejection remains stable from no ECEM tower threshold to a threshold value of 5GeV. For a 10GeV threshold, although the rejection increases (not shown in figure), the efficiency becomes small.

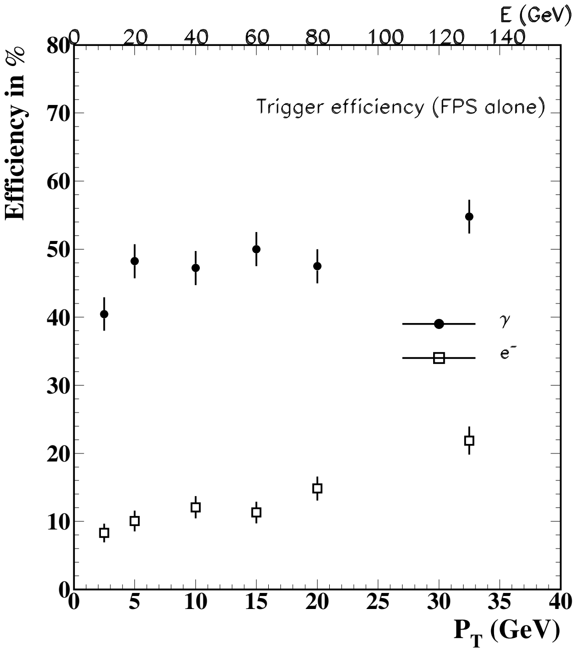

Figure 4.25: *Efficiency of the photon trigger as function of the transverse momenta of the particles.*

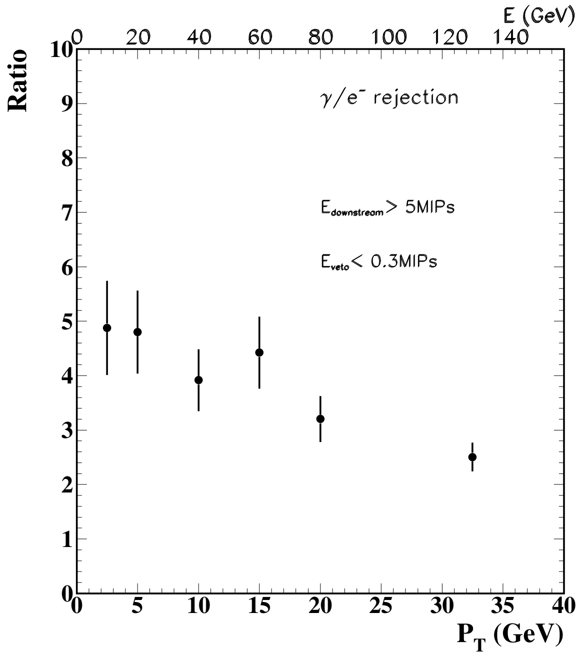

Figure 4.26: *Photon versus electron rejection factor as a function of the transverse momenta.*

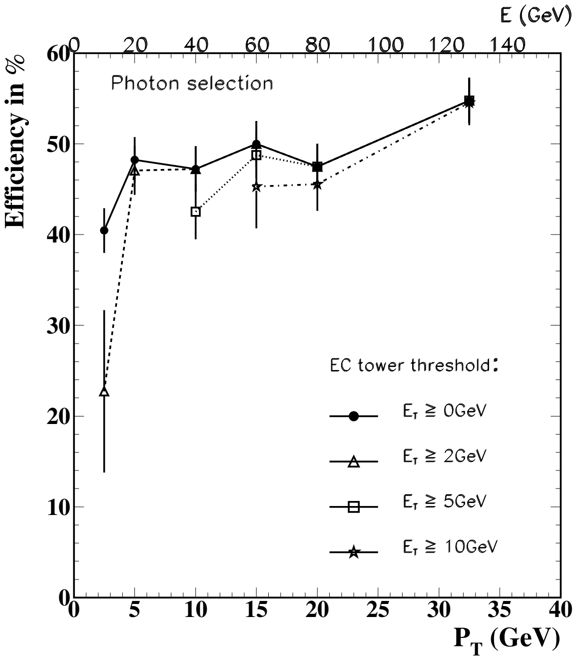

Figure 4.27: *Dependence of photon efficiency on EM trigger tower thrshold.*

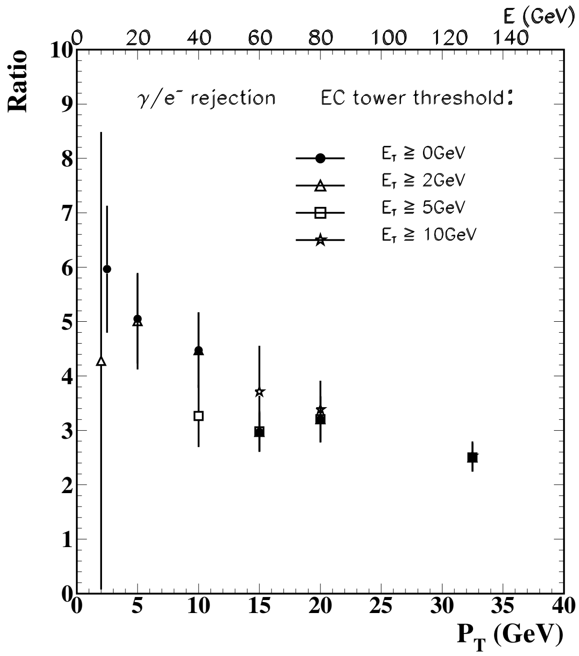

Figure 4.28: *Dependence of photon versus electron rejection factor on EM trigger tower threshold.*

5 Trigger rates and occupancy at Level-1

The QCD production cross-section is highly dominant at the TeVatron, since one observes a factor of (at least) 50,000 between QCD dijets production cross-sections and W or Z bosons cross-sections. These events, which are likely to trigger via EM deposition(s) in the calorimeter and/or the FPS detectors, therefore require a careful estimation of their trigger rates.

We first recall the expected cross-section for QCD dijets events in several $\mathrm{P_T}$ ranges. The expected number of extra interactions per crossing for run II at $\mathcal{L} = 2 \times 10^{32} cm^2 s^{-1}$ is presented as well. These two factors make the dijet events a significant source of background for the Electro-Magnetic object triggers.

The occupancy as measured in the FPS layers are reported in the following section. Then selection rates are computed for the SNG_ELE (single electron) as well as for the SNG_EM (single EM = ELE+GAM) triggers. At L1, given the high level of QCD background, only the combination of signals from the EC and the FPS is relevant. We investigate several combinations of these information, going from a crude coincidence of an EC signal with a FPS signal per side (N/S), to tighter requirement (per quadrant or octant). We present here the results of this investigation.

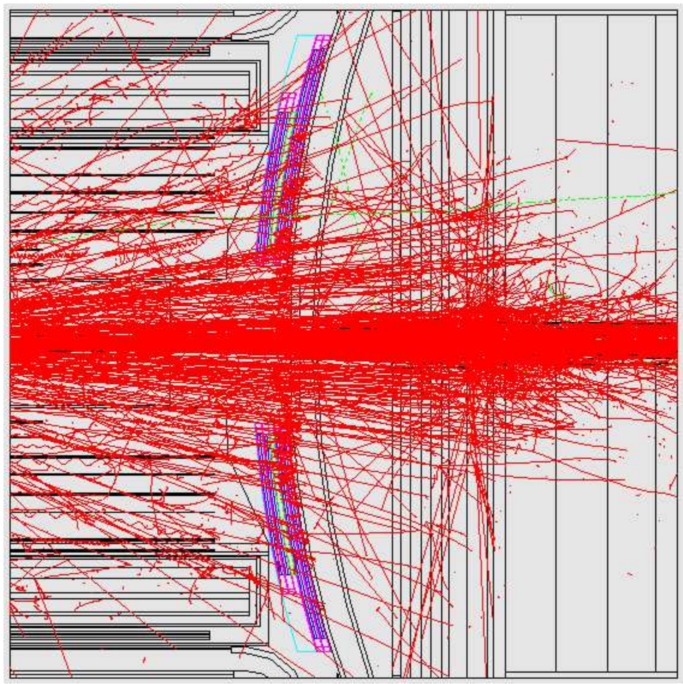

Figure 5.29: *Transverse view of a dijets events overlaid with 6 mbias interactions. These events are simulated with low P_T ISAJET dijets. No E_T cut is applied here.*

5.1 Dijet cross-sections and MinBias interactions at run II

5.1.1 Dijet cross-sections

Dijet cross-sections are taken from the ISAJET generated outputs. They have been computed for 5 P_T intervals ranging between 2 and 500 GeV. They are reported in table 4. These numbers have been used to compute the trigger rates in the following section.

Range in P_T	σ (μb)
02-10 GeV/c	56,590
10-20 GeV/c	543.0
20-40 GeV/c	37.3
40-500 GeV/c	1.8

Table 4: *Dijet Cross sections from samples generated with ISAJET. Dijets have been produced with the CTEQ pdf.*

5.1.2 Number of minimum bias interactions

The number of extra interactions per crossing depends on the luminosity as well as on the number of bunches circulating in the TeVatron. This number, which follows a Poisson distribution, depends on the luminosities and the bunch configuration. They have been computed by Chris Klopfenstein [7] for different luminosities and are reported in table 5 for a luminosity of 2×10^{32} cm^{-2}.s^{-1} and 36/99 bunches.

N(int)	36 bunch	99 bunch
0	0.00421672	0.13688453
1	0.02305996	0.27221098
2	0.06305397	0.27066177
3	0.11494105	0.17941425
4	0.15714448	0.08919658
5	0.17187515	0.03547558
6	0.15665555	0.01175789
7	0.122386	0.00334028
8	0.08366151	0.00083032

Table 5: *Probability for a number of interactions per crosssing determined using a Poisson distribution. The luminosity is 2×10^{32} $cm^{-2}.s^{-1}$ for two bunch configurations. Calculations have been performed by C. Klopfenstein. The average number of extra interactions is 2 for 99 bunch configuration.*

Thus, for a 99 bunch configuration, 59% of the events are produced with more than 2 extra interactions per crossing. Among them, only 14% will be overlapped with more than 4 extra interactions. On average, two extra interactions are superimposed to the events.

5.2 Occupancy at L1 in the FPS

5.2.1 Occupancy for 2 mbias interactions per crossing

The occupancy was determined by using di-jet events with $2 < P_T < 500$ GeV overlaped with two, four and six additional minimum bias interactions.

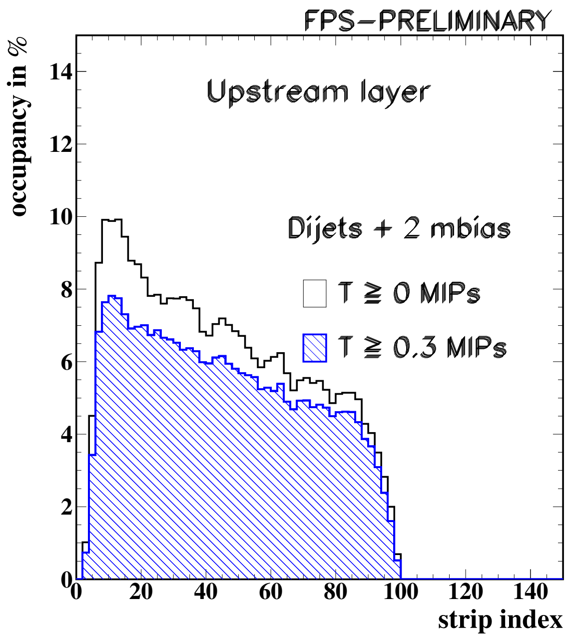

Figure 5.30: *Occupancy for the layers in front of the lead converter (MIP layer) for a threshold of T = 0 MIP and T = 0.3 MIP .*

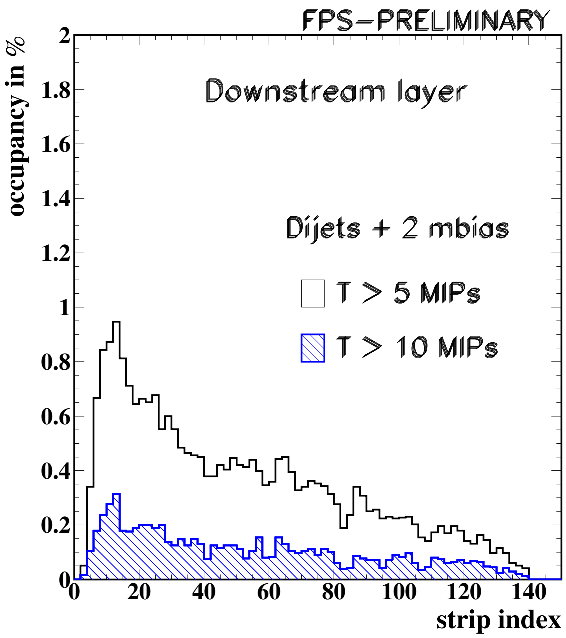

Figure 5.31: *Occupancy for the layers behind the lead converter (shower layer) for two thresholds: T= 5 MIPs and T= 10 MIPs.*

Typically, the population of hits is concentrated around the beam pipe, as expected from the QCD cross-section. The probability that a strip is struck with an energy above standard thresholds (0.3 MIP upstream, 5 MIPs downstream) gives a good indication of the average number of fake candidates spawned by QCD background.

Fig. 5.30 and Fig. 5.31 show the probability that a strip is hit, respectively in the front layers and in the shower layers for different thresholds. As expected the occupancy is function of the η-dependence of the QCD cross-section. In the front layer, the occupancy is below 8.0% for a 0.3 MIP threshold. This means that about 8 strips per layer (u or v) pass the trigger threshold per module for dijet+2 mbias events. Downstream, occupancy is shown for two different thresholds at T= 5 MIPs and T=10 MIPs. For a threshold set at 5 MIPs, the occupancy is found well below 1.0% per layer (u or v).

5.2.2 Dependence in the number of interactions

The dependence of the results in the number of extra interactions has been investigated. Fig. 5.32 and 5.33 display the occupancy in % computed from dijets events overlaid with 0,2,4 and 6 mbias interactions, respectively, for the MIP and the shower layers.

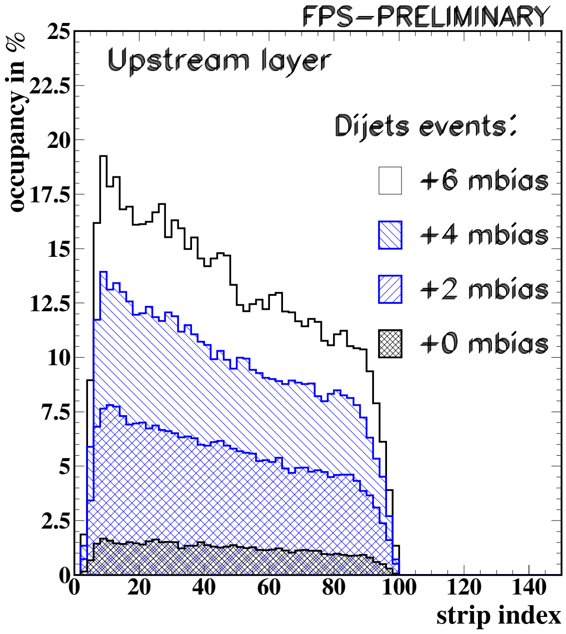

Figure 5.32: *Occupancy for the layers in front of the lead converter (MIP layer) for a threshold T = 0.3 MIP. Occupancy for dijets with 0, 2,4 and 6 overlaid mbias events are compared.*

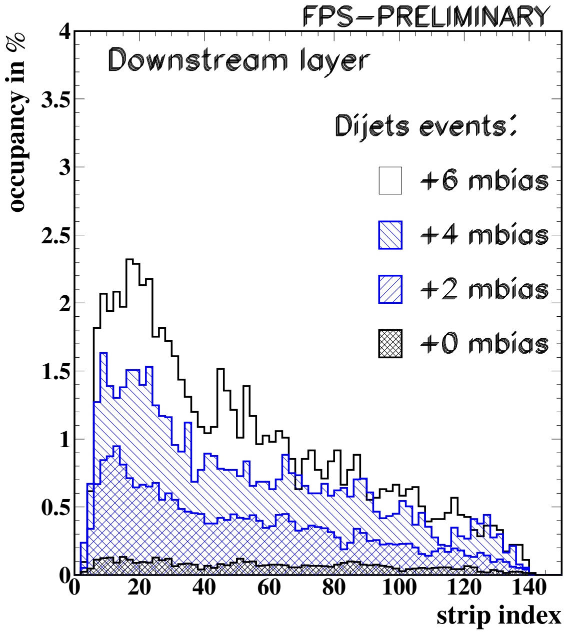

Figure 5.33: *Occupancy for the layers behind the lead converter (shower layer).for a threshold T = 5 MIPs. Occupancy for dijets with 0, 2,4 and 6 overlaid mbias events are compared.*

With thresholds set at 0.3 MIP for the front layers and 5 MIPs for the shower layers, we observe that the occupancy in the 4 layers is very sensitive to the number of extra interactions: from 1.3% (0 mbias) this number is increased to 19% for 6 mbias. On the other hand, as for the shower layer, occupancies do not exceed 2.5 % in the worst case. It should be reminded here that the probability to observe more than 4 extra interactions is about 14% in the 99-bunch configuration.

One can compute the mean occupancy per module for the layers in front of the lead or behind the converter. The dependence in the number of extra interactions N may then be described by the following law:

$$< \mathrm{Occ}^{\mathrm{mip}}(\mathrm{N}) >= 1.34\% + \mathrm{N} \times 2.37\%$$

in the MIP layers, whereas one observes the following dependence:

$$< \mathrm{Occ}^{\mathrm{shower}}(\mathrm{N}) >= 0.08\% + \mathrm{N} \times 0.17\%$$

in the shower layers. These results are justified in Fig. 5.34 and presented in table 6.

The global average occupancy is given by the mean occupancies computed for N going from 0 to 8 weighted by the appropriate Poisson coefficient. These coefficients are reported in table 5. The following average mean occupancy are expected for the run II:

$$< \mathrm{Occ} >= 6.1\% \ \ \text{upstream at } \mathcal{L} = 2 \times 10^{32}\mathrm{cm}^2.\mathrm{s}^{-1} \text{ and 99 bunches}$$

and

$$< \mathrm{Occ} >= 0.4\% \ \ \text{downstream at } \mathcal{L} = 2 \times 10^{32}\mathrm{cm}^2.\mathrm{s}^{-1} \text{ and 99 bunches}$$

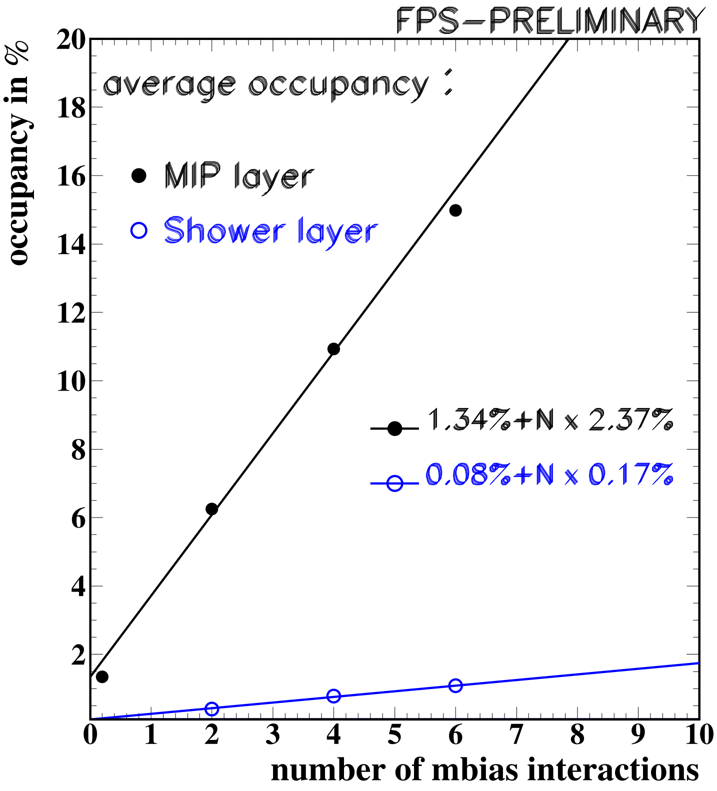

Figure 5.34: *Averaged occupancy in the MIP layers (black dot) and in the shower layer (open dot) as a function of the number of extra interactions.*

Results are about equal to what we expect for 2 extra interactions per crossing. They imply that about 8 strips per module will pass the low threshold in the MIP layers (195 per event for the two-sided detector), whereas less than one strip per module is seen in the shower layer (18 per event). We note that no coincidence between upstream and downstream deposition have been required for the present calculation.

N(int)	Occupancy	
per crossing	MIP layer	Shower layer
1	3.71%	0.25%
2	6.08%	0.42%
3	8.45%	0.59%
4	10.82%	0.76%
5	13.19%	0.93%
6	15.56%	1.10%

Table 6: *Occupancy as expected in the FPS detector for various number of interactions per crossing. The average number of extra interactions expected for* $2 \times 10^{32}\mathrm{cm}^2.\mathrm{s}^{-1}$ *and 99 bunch configuration is 2.*

5.3 Single electron trigger: SNG_ELE

The di-jets samples described in section 5.1.1 have been used in this study. The single electron trigger, denoted SNG_ELE, is based on the combination of signals coming from both the FPS detector and the EM part of the End Calorimeter (EC). Because of timing constraint at L1, only the sum of the EM trigger towers over a side, a quadrant or an octant is available at the L1 trigger manager level. First, we compute the SNG_ELE trigger rates for the three different combinations of FPS and EC information. Then the dependence of the rates in the FPS threshold is studied.

5.3.1 Combination of FPS and EC information at L1

We use the electron SNG_ELE trigger rates to have been computed for various types of combination of the FPS and the EC EM towers.

1. Confirmation of an EM tower with a FPS signal located in the same side (N/S) (corresponding to the sum of the 16 "phi-sectors")

2. Confirmation of an EM tower with a FPS signal located within the same quadrant of the EC (corresponding to the sum of 4 "phi-sectors")

3. Confirmation of an EM tower with a FPS signal located within the same octant of the EC (sum of 2 "phi-sectors")

Table 7 reports the results compared for the three cases for $\mathrm{E_T}$ = 2 GeV, $\mathrm{E_T}$ = 5 GeV and $\mathrm{E_T}$ = 10 GeV EM thresholds, while a threshold of T = 5 MIPs was set for the FPS.

EM Threshold	$\mathrm{E_T} \geq 2$ GeV	$\mathrm{E_T} \geq 5$ GeV	$\mathrm{E_T} \geq 10$ GeV
EC alone (0)	240,810 Hz	5,760 Hz	690 Hz
FPS + EC (1)	28,410 Hz	5,340 Hz	470 Hz
FPS + EC (2)	20,540 Hz	3,610 Hz	280 Hz
FPS + EC (3)	18,420 Hz	3,430 Hz	260 Hz

Table 7: *Trigger rates for four combinations of FPS and EC information: a EM tower is required (0) to pass E_T threshold (1) to be confirmed by a FPS signal located on the same side (2) to be confirmed by a FPS signal located within the same quadrant (3) to be confirmed by a FPS signal located within the same octant. FPS thresholds are set to 0.3 MIPs upstream and 5 MIPs downstream. Luminosity is $\mathcal{L} = 2 \times 10^{32}\mathrm{cm}^2.\mathrm{s}^{-1}$ All rates are computed for dijet events overlaid with 2 minbias interactions.*

As a conclusion, the finer the matching with the EC signal, the better the rejection rate is. The combination of the quadrant EC with the FPS signal brings an improvement of a factor 2.5 for $E_T \geq 10\ GeV/c$ with respect to the EC alone. However the use of the octant does little in additional rate rejection (2.6). A reasonable choice therefore is to use the quadrant information at L1.

5.3.2 SNG_ELE trigger rates

Fig. 5.35,5.36, 5.37 and 5.38 display the transverse energy ($\mathrm{E}\times\sin\theta$) as measured in a EC tower from 02-10, 10-20, 20-40 and 40-500 GeV/c dijet events overlaid with 2 MinBias interactions. As expected the distributions are peaked at very low energy values, around 500 MeV/c. Most of the selected candidates come from high energy samples, with relative weight given by the ratio of the cross-sections reported in table 4.

Table 8 reports the trigger rates measured with the EC alone (first row) and with the combination of a FPS signal with a EM tower fired in the same quadrant (next rows).

Threshold in EC	$\mathrm{E_T} \geq 2$ GeV	$\mathrm{E_T} \geq 5$ GeV	$\mathrm{E_T} \geq 10$ GeV
EC alone	240,810 Hz	5,760 Hz	690 Hz
EC + FPS (T=5 MIPs)	20,540 Hz	3,610 Hz	280 Hz
EC + FPS (T=10 MIPs)	9,120 Hz	1,920 Hz	160 Hz

Table 8: *Electron trigger rates computed on di-jets+2 MinBias events using the EC calorimeter alone (1^{st} row) or combining the FPS and EC trigger tower within the same quadrant (2^{nd} and 3^{rd} rows). FPS thresholds are set to 0.3 MIPs upstream and 5 MIPs or 10 MIPs downstream. Luminosity is* $\mathcal{L} = 2 \times 10^{32}\mathrm{cm}^2.\mathrm{s}^{-1}$

In the first row, an event is selected if at least one EM trigger tower is fired with a transverse energy above 2, 5 or 10 GeV. In the second case, we match the signal in the End Calorimeter with the the signal from the FPS modules located within the same quadrant, each quadrant covering an angular region corresponding to 4 FPS modules.

Fig. 5.39 displays the SNG_ELE trigger rates as function of the EM tower threshold. The rates obtained for a low $\mathrm{E_T}$ threshold in the calorimeter are obviously unacceptable. If one aimed to trigger on $J/\Psi \rightarrow e^+e^-$ issued from b-quarks without applying a huge pre-scaling factor, a single electron trigger turns out to be problematic.

For higher EC towers thresholds, rates of 700 Hz are observed in the Forward region if the EC alone is used. For $\mathrm{E_T} = 10$ GeV threshold, a reduction by a factor 2 is reached at level-1 by requiring the coincidence of a fired EM tower and a FPS candidate located within the same quadrant. Rates of 280 Hz are observed. This energy range typically corresponds to the W/Z bosons physics scale.

As to the dependence on the FPS high threshold, one notices that the use of a FPS-threshold twice as much as the one finally chosen (T=5 MIPs) results in a reduction by an additional

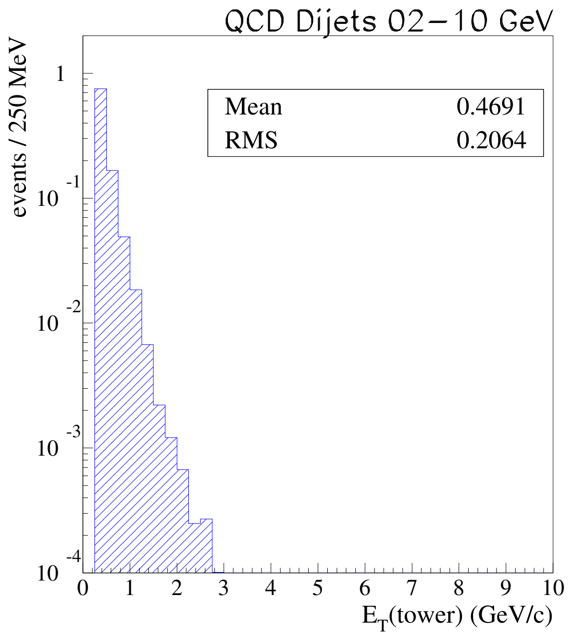

Figure 5.35: *Transverse energy as measured in a ECEM tower for 2-10 GeV/c dijets.*

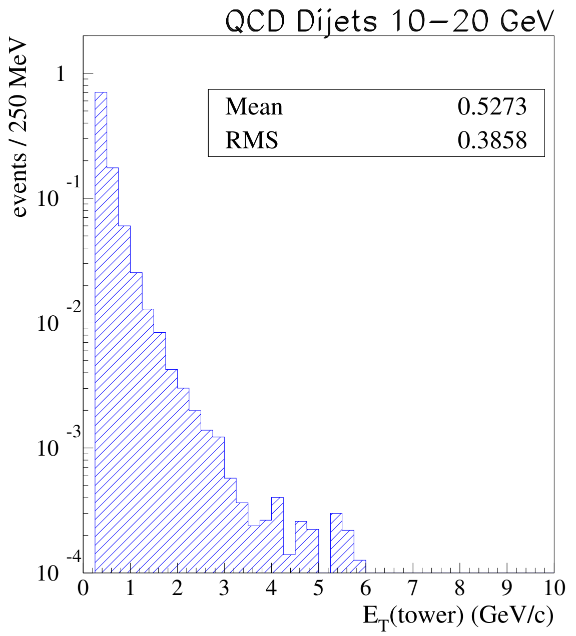

Figure 5.36: *Transverse energy as measured in a ECEM tower for 10-20 GeV/c dijets.*

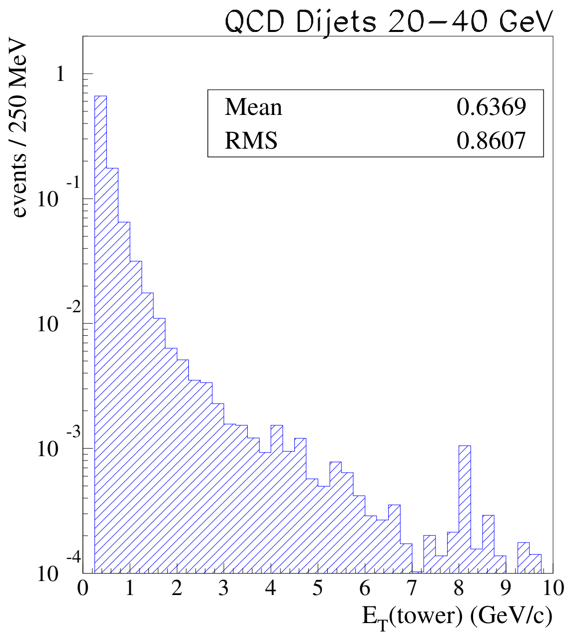

Figure 5.37: *Transverse energy as measured in a ECEM tower for 20-40 GeV/c dijets.*

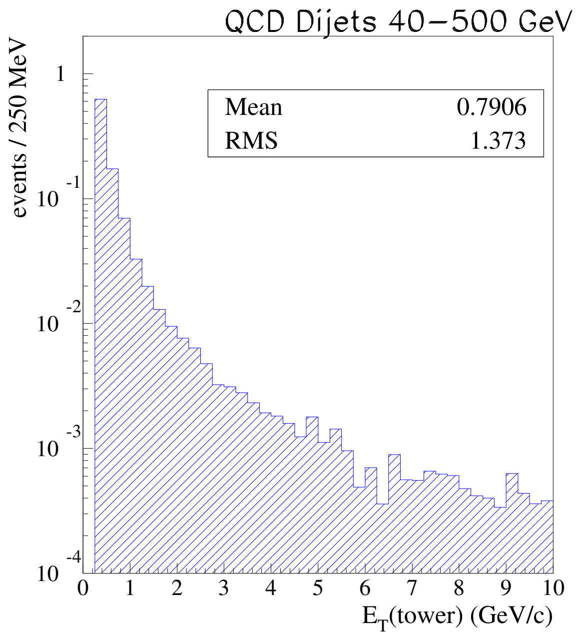

Figure 5.38: *Transverse energy as measured in a ECEM tower for 40-500 GeV/c dijets.*

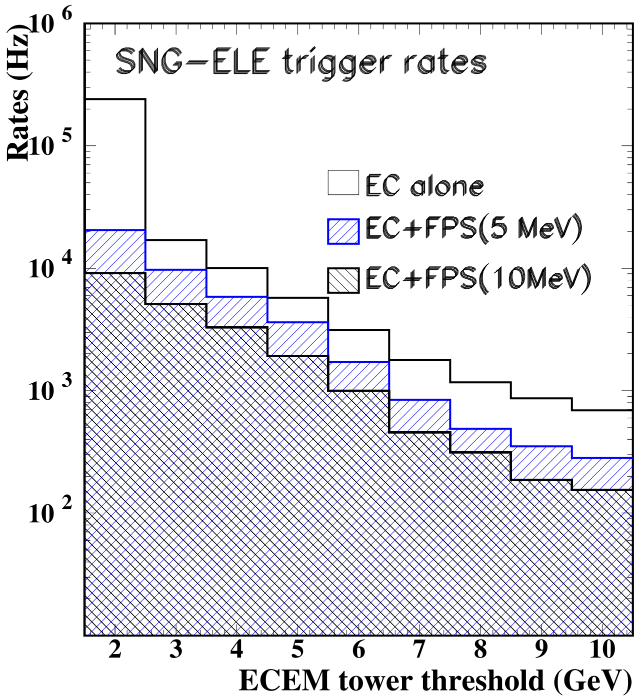

Figure 5.39: *Single electron (SNG_ELE) trigger rates computed with dijet samples + 2 mbias interactions generated over a range from 2 to 500 GeV for: (1) EM tower in the EC trigger. (2) EM tower + FPS with 5 MIPs threshold and (3) EM tower + FPS with 10 MIPs threshold*

factor 1.7 of the trigger rates (last row of table 8). The only purpose of our preference for a 5 MIPs threshold was to keep the capability of the detector to trigger efficiently on low P_T electrons: 85% are selected with a 5 MIPs threshold against 50% with 10 MIPs.

5.4 Single EM trigger: SNG_EM

The single EM trigger, denoted SNG_EM, is based on the same combination of signals coming from the FPS detector and the ECEM tower that was described for the SNG_ELE trigger. However here rates have been computed for the sum of the ELE and GAM candidates for different ECEM E_T threshold.

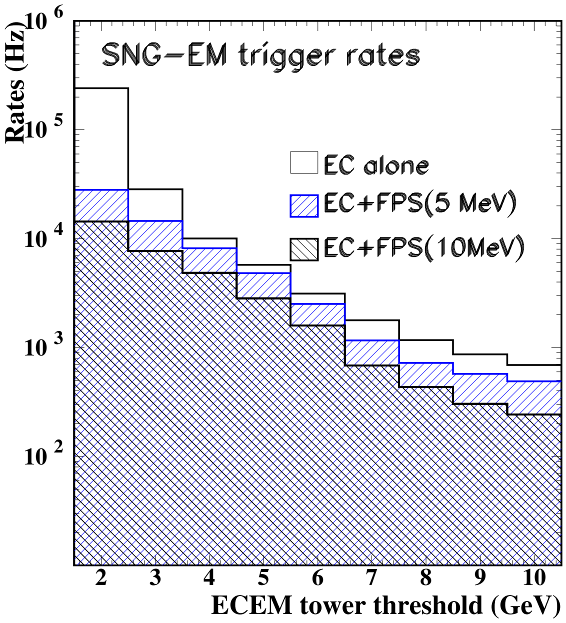

Figure 5.40: *Single EM (SNG_EM) trigger rates computed with dijets samples + 2 mbias interactions generated over the range 2 to 500 GeV for: (1) EM tower in the EC trigger. (2) EM tower + FPS with 5 MIPs threshold and (3) EM tower + FPS with 10 MIPs threshold*

Fig. 5.40 displays the rates as obtained from the ISAJET di-jets as function of the ECEM threshold. The sensitivity to the FPS downstream threshold is shown on the plot by the two curves obtained for a downstream threshold set at 5 or 10 MIPs. Table 9 reports the expected rates for $E_T = 2, 5$ and 10 GeV ECEM thresholds.

Threshold in EC	$E_T \geq 2$ GeV	$E_T \geq 5$ GeV	$E_T \geq 10$ GeV
EC alone	240,810 Hz	5,760 Hz	690 Hz
EC + FPS (T=5 MIPs)	28,140 Hz	4,830 Hz	490 Hz
EC + FPS (T=10 MIPs)	14,310 Hz	2,840 Hz	240 Hz

Table 9: *Electron trigger rates computed on di-jets + 2 MinBias events using the EC calorimeter alone (1^{st} row) or combining the FPS and EC trigger tower within the same quadrant (2^{nd} and 3^{rd} rows). FPS thresholds are set to 0.3 MIPs upstream and 5 MIPs or 10 MIPs downstream. Luminosity is* $\mathcal{L} = 2 \times 10^{32} \mathrm{cm}^2.\mathrm{s}^{-1}$.

5.5 Di-electron trigger: DBL_ELE

Table 10 reports the trigger rates measured with the EC alone (first row) and with the combination of a FPS signal with a EM tower fired in the same quadrant (next rows) for di-electron candidates. No requirement on the location or the opening angle between the two depositions has been asked. Such trigger algorithm may be used to detect at an early stage electron coming from prompt J/ψ or J/ψ produced in b-hadronic decays. More extensive study is currently under working.

Threshold in EC	$E_T \geq 2$ GeV	$E_T \geq 3$ GeV	$E_T \geq 4$ GeV	$E_T \geq 5$ GeV
EC alone	34,600 Hz	15,280 Hz	9,020 Hz	4,580 Hz
EC + FPS (T=5 MIPs)	5,900 Hz	4,440 Hz	4,400 Hz	2,520 Hz
EC + FPS (T=10 MIPs)	820 Hz	580 Hz	520 Hz	240 Hz

Table 10: *Di-Electron trigger rates computed on di-jets events using the EC calorimeter alone (1st row) or combining the FPS and EC trigger tower within the same quadrant (2nd and 3rd rows). FPS thresholds are set to 0.3 MIPs upstream and 5 MIPs or 10 MIPs downstream. Luminosity is* $\mathcal{L} = 2 \times 10^{32}\mathrm{cm}^2.\mathrm{s}^{-1}$. *All samples have been overlaid with 2 minbias interactions.*

As we intend to detect low P_T electrons, the rates have been computed for E_T thresholds ranging between 2 and 5 GeV/c. Results show rates from 800 Hz at $E_T \geq 2$GeV/c to 250 Hz at $E_T \geq 5$ GeV/c. Efficiency and more sophisticated algorithms are studied in a note under preparation.

6 L1 and L2 electronics

In this section, we describe the status of the L1 and L2 data path from the Front End (FE) to the Trigger Managers (TM), given our current knowledge of the electronics design, described in [6].
We first briefly present the design of the readout system used to route the signal from the strip fibers to the FE board.

The L1 logic takes place partly in the FE board where each ϕ-sector is treated independently and in the Trigger Manager (TM) crate, where all information is regrouped. This is the place where the L1 global decision is taken.
In this context, we present the information that we intend to transfer from the FPS FE to the L1 trigger manager (TM). The size (bit counts) and the time needed to form and transmit L1 objects are evaluated with respect to the 4.2μs time constraint.

In the final sub-section, we briefly review the current status of the L2 trigger design. We define the role of a Pre-processor level as well as the one taken by the global level.
So far, the trigger objects that we intend to use at the L2 are based on the digital information. Preliminary studies show that the use of the full information (analog) at that level does not bring any significant improvement in the trigger performance. However the option of using the analog information is not yet definitely ruled out and studies are still under way.

6.1 Readout scheme and electronics for the FPS trigger

The design of the electronics readout system is based on the use of SIFT chips also used for the Fiber Tracking detector. They are described in [4]. A detailed description of the signal routing may be found in [3]. However, it is worthwhile to discuss the readout system for a better understanding of the L1 trigger algorithm. We should also keep in mind that for the FPS we are adapting a readout system which was primarily designed for detecting MIP like signals in tracking detectors.

Clear optical waveguides route the signal from the FPS modules to the visible light photon counter (VLPC) cassettes. One scintillator from the detector couples to one channel in the VLPC. Here, the light signal is converted to electrical signal with high quantum efficiency ($\sim$80%) and high gain ($\times$40,000). Fig. 6.41 shows a schematic of a VLPC cassette along with the associated front end electronic (FE) boards. There are 1024 channels to a VLPC cassette which are evenly divided between two FE boards. The signal from the detector at L1 is divided into 22.5^0 ϕ sectors which we call a readout-sector. A readout-sector sums the signals emerging from both a small (upstream) and a large (downstream) module (a total of 4 layers) at the same ϕ position. These signals are grouped and sent to one FE board, for a total of 482 channels per board. This is also expected to simplify the L1 trigger as it will have to act on a single board for each sector taking into account all the 4 layers of the small and large modules in that

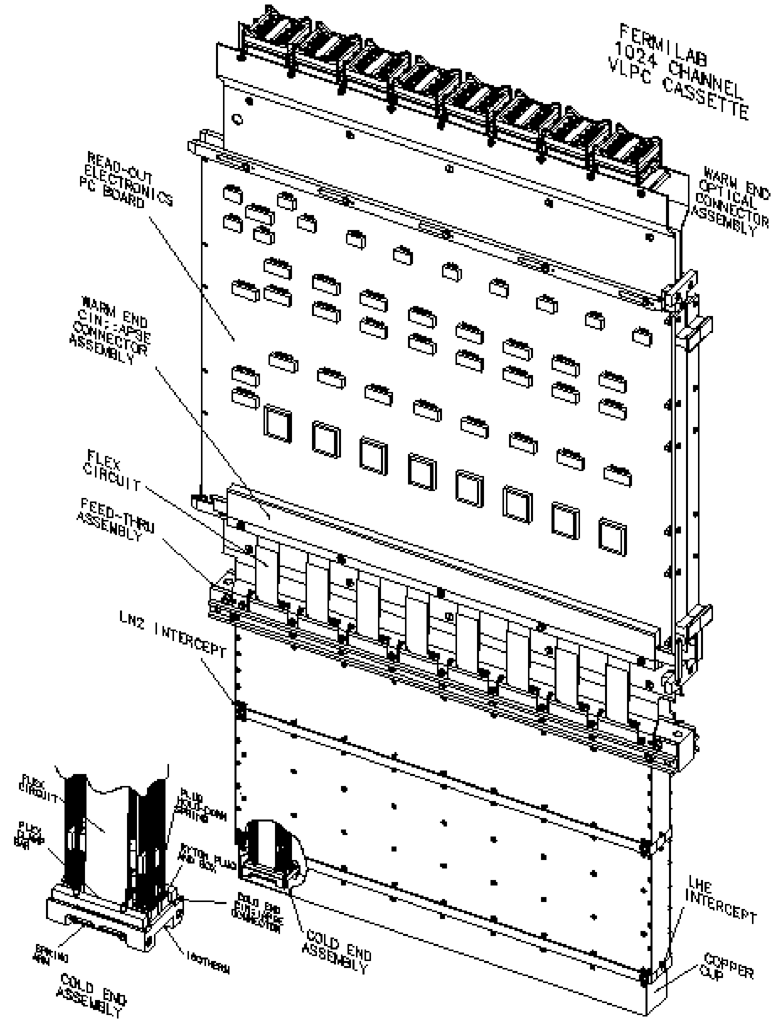

Figure 6.41: *VLPC cassette.*

sector.

The schematic of the readout system is shown in Fig. 6.42. The VLPC has an output of 100fC/MIP. In order for the system not to saturate very frequently, a fraction of this charge is drained away before input to SIFT chips. The signal from each VLPC channel is then further charged divided into two analog outputs with a ratio of 10:1 (high and low gains, respectively) through capacitive coupling. These outputs feed two distinct Multi-Chip Modules (MCM) designated as 10$\times$MCM and 1$\times$MCM. Each of these arms has its own scintillating fiber tracker (SIFT) chip and SVX-II readout chip. There are twice as many SIFT and SVX channels as there are input channels.

The SIFT chips provide a fast trigger signal and also drives an analog signal to an SVX-II chip. Each SIFT chip contains a dual range discriminator for which a threshold may be set in any run, downloadable in a predetermined ranges of values ([5,50]fC or [30,300]fC). The high

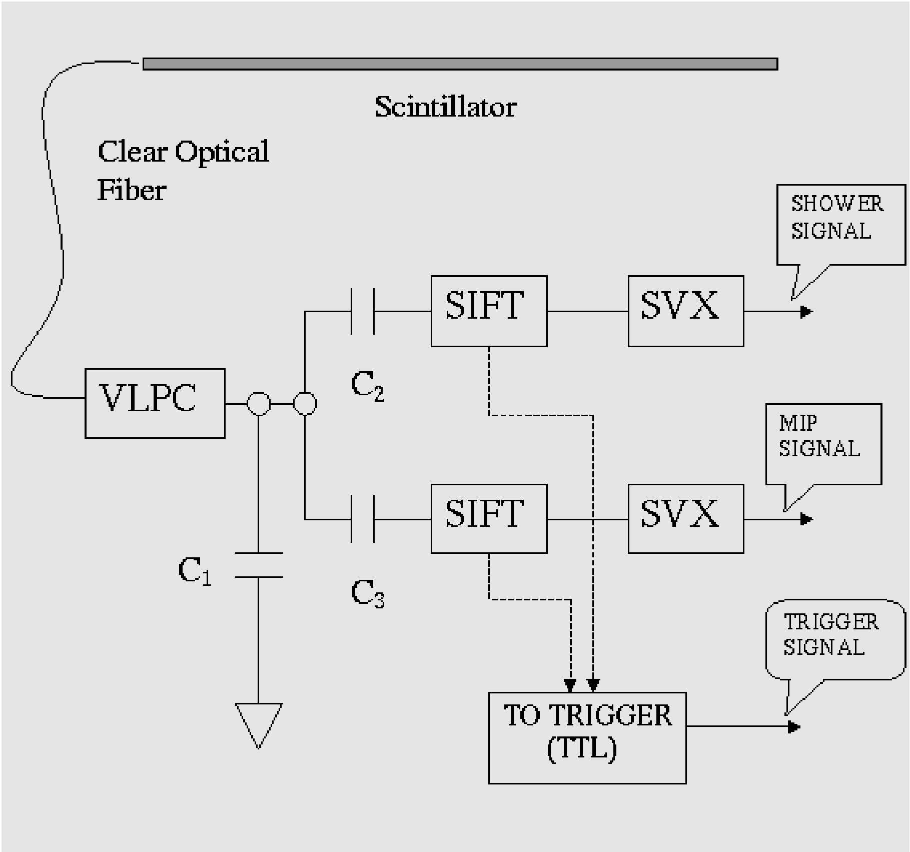

Figure 6.42: *FPS Readout scheme*

gain arm is used to detect MIP like deposits while the low gain arm is used to detect large shower energies.

From the noise point of view, the random noise in a SIFT has a width of ~0.7fC. Taking a generous 7σ above this as a reasonable trigger threshold, one gets a minimum trigger threshold of 5fC. This implies that in the high gain arm, one would like to have a trigger threshold for MIPs roughly at 5fC. Hence, at the input to the SIFT, the charge has to be divided in such way that the high gain arm has fine enough resolution to resolve individual MIP peaks above the noise threshold, while the low gain arm has enough dynamic range to accomodate large shower energies.

Trigger pickoff signals are then fed into a series of Large Field Programmable Gate Arrays (FPGA) located on the FE board. The gate arrays are pre-loaded with the logic defined to form clusters. The trigger logic for each module is thus self-contained on each Front End board, all the channels of a four layer trigger being contained on each board.

6.2 L1 logic and data path

The L1 logic takes place at the FE board, where objects from a ϕ-sector are formed, and at the L1 TM, where the number of objects is counted and sorted by quadrant to perform the matching with the ECEM information. An overview of the L1 scheme is displayed in the schematic Fig. 6.43.

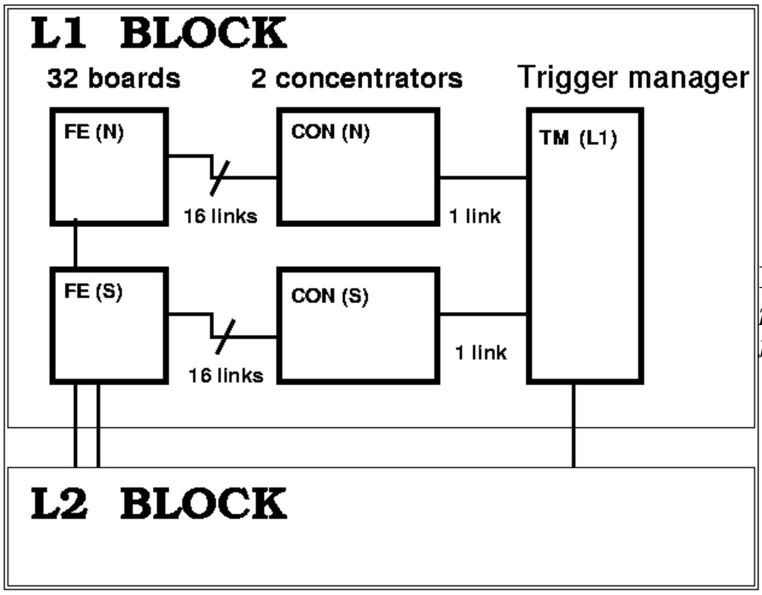

Figure 6.43: *Schematic of the L1 data path. All details on the links may be found in [6].*

6.2.1 L1 Objects and data transfer to the L1 TM

As seen previously, the L1 logic (FPGA) is partly contained in the VLPC FE board. Each board receives 482 readout channels that correspond to the number of strips of a ϕ-sector, ie: 2 u- layers and 2 v- layers. At this stage, the number of EM = ELE.OR.GAM candidates is counted separately for the u- and the v- layers the following way: in the shower layers, each time a strip passes the threshold, confirmation of hit upstream in the appropriate window is checked (ELE or GAM); also each time two adjacent strips pass the threshold (and are of the same type, ie: ELE or GAM) the cluster width is incremented and the number of cluster(s) kept unchanged. Scanning of all downstream strips result in the number of clusters with their size, type (ELE/GAM) and orientation (U/V).

The information that needs to be transferred from each FE board to the L1 TM is the number of such clusters with their orientation, their type as well as their ϕ-location (1 out of 4 quadrants). The ϕ-location and the side (N/S) information is carried by the cable ID. The size of the objects routed to and treated at the L1 TM is reported in table 11. Each cable linking the FE board to the TM can carry up to 96 bits. This means that a maximum of 12 u- and v- 2-bits clusters per ϕ-sector may be sent given that both the ϕ-sector and the side index are

L1 object (TM)	Size in bit(s)
Cluster orientation (U/V)	1 bit
Cluster type (ELE / GAM)	1 bit
TOTAL	2 bits
Info carried by CABLE	
Φ-sector (1 to 4) [cable]	2 bits
Side N/S [cable]	1 bit

Table 11: *Object transferred to the L1 Trigger Manager and size in bits. Each object sent from each FE to the TM has a size of 2-bits, while the ϕ-sector and side information of the cluster are identified by the cable. See the text for the role of the concentrator.*

identified by the cable index. From the physics simulation point of view, this is far more than the worst expectations.

The global structure involves eight VLPC cassettes per side of the FPS, corresponding to 16 FE boards. Signals are brought from the FE board to a concentrator (CON) through 16 cables per side. Altogether for the entire detector, there are 32 such cables and 2 Concentrator boards (one per side). The side and the quadrant from which the data has come is identified by the cable. The Concentrator board sums the sectors into quadrants and sends the sums to the L1 trigger manager (TM). There is one cable per side (N/S) for this transfer from the concentrator to the L1 TM.

6.2.2 Number and width of clusters for physical events

The average number and width of clusters produced by an electron+2MinBias event and dijet+2MinBias event in the FPS in any one of the shower layers has been studied using Monte Carlo samples.

Fig. 6.44 and 6.45, shows these plots for the sector struck by the electron for 10GeV & 130GeV single electrons overlaid with 2 minimum bias events. This is for the u- layer (similar for the v- layer). The shaded histogram shows quantities calculated with a 5MIPs threshold on the signal in shower layers while the open histogram is for a 10MIPs threshold. The average cluster width increases with increasing electron energy. However, it decreases with increasing threshold. With the 5MIPs threshold, there are about 1.2 clusters/electron in the struck sector and in about 14-20% of the events there is an additional electron cluster. When the upstream MIP requirement is dropped, another $\sim$14-20% of the events show an additional γ cluster. Thus, in the sector hit by the electron, two clusters (one u- & one v-) are found along with a third accidental cluster. However, when we take into account the dijets, the situation changes further.

Compared to the electron clusters, the accidental clusters produced by dijets overlayed with 2 minimum bias events are narrower as can be seen from Fig. 6.46 and 6.47. On the average, we see 1.09-1.22 clusters per side of the FPS per event. In more detail, for low E_T (2-10GeV) dijets we see $\sim$1.09 clusters/side/event which increases to $\sim$1.22 clusters/side/event for higher E_T dijets (20-40GeV). Taking these clusters into consideration, we have 2 more clusters

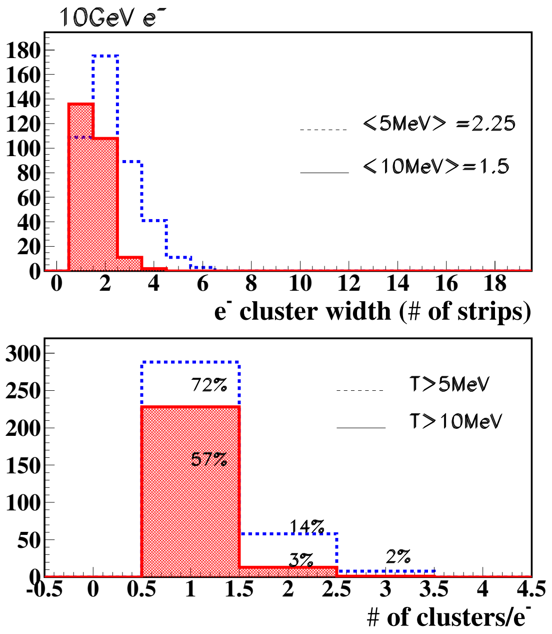

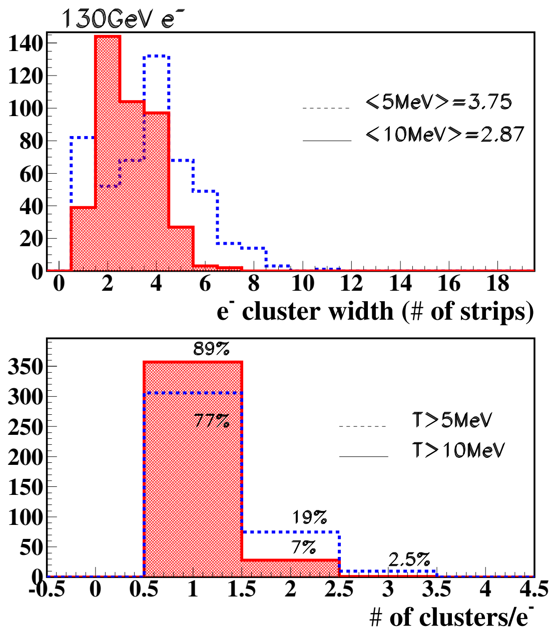

Figure 6.44: *Cluster width & number of clusters in FPS for 10GeV e^- +2MinBias events*

Figure 6.45: *Cluster width & number of clusters in FPS for 130GeV e^- +2MinBias events*

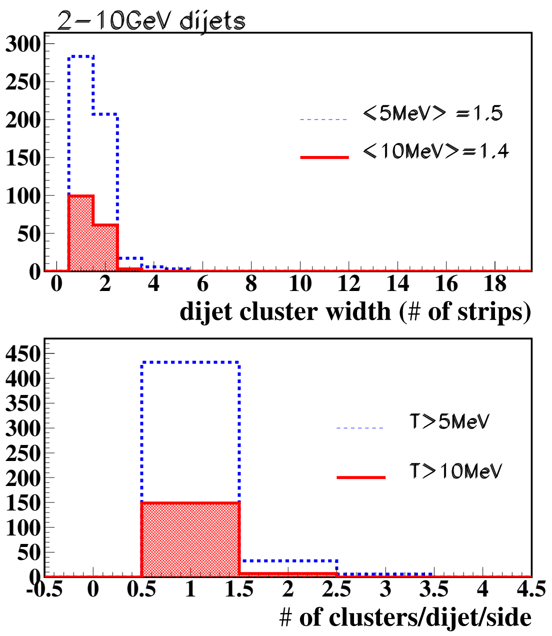

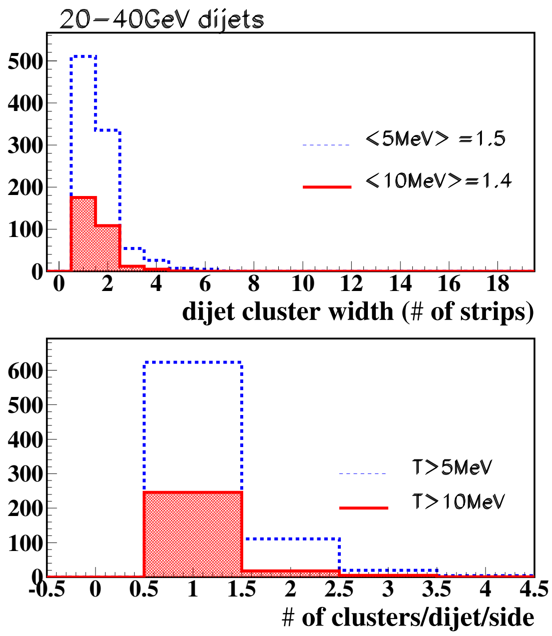

Figure 6.46: *Cluster width & number of clusters in FPS for 2-10GeV dijet$^-$ +2MinBias events/side/event*

Figure 6.47: *Cluster width & number of clusters in FPS for 20-400GeV dijet$^-$ +2MinBias events/side/event*

(one/layer) to add to the electron clusters/event. So, in both u- & v- together, we will have 4-5 clusters/event for an electron per side.

6.2.3 L1 Algorithm timing

The time needed to make a decision with the L1 algorithm has been determined. It is expected that one crossing (132 ns) will be needed to get the information from the VLPC to SIFT and to the FPGA. It will then take 2 to 4 crossings to form clusters in each layer by matching downstream hits with upstream MIP/VETO requirement and forward the count of these candidates to a single FPS L1 manager. This manager will then require another 1 to 4 crossings to sort the Front End data, form and send the trigger terms to the L1 trigger framework. Thus a conservative estimate of the time needed to make a decision at this level is 9 crossings or 1.2 μs. The time needed for the signal to be transferred from the calorimeter to the trigger manager will take 5 crossings and the matching between the FPS and the calorimeter signal is expected to take an additional 5 crossings, which totals to 1.3 μs. This gives a total time of ~ 2.6 μs, which is compatible with the limit of 4.2μs.

These results make possible the use of trigger signals from the calorimetric trigger tower at L1. However due to timing and hardware constraints, only the sum over towers in each quadrant of the calorimeter endcap is available. The information should be available within 5 crossings.

6.3 From L1 to L2

A note in preparation [8] is devoted to the description of the L2 algorithm. Here we just give indications of what we think the L2 should be able to handle in terms of data load.
The L2 will make a decision based upon the L1 trigger. As we intend to do a fine matching of the FPS clusters with the ECEM trigger tower at the L2 global (L2GLB), we need here to collect more information concerning the clusters. This is why the L2 uses the digital information provided by the SVX-II chips located in the VLPC boards.

6.3.1 L2 structure and role

The schematic 6.48 drafts the structure of the L2 we intend to use. All details concerning the design and specifications are reported in [4]. Basically the L2 data path involves two steps: the first is based on a set of Pre-processors which will re-format the data sent from the FE board, so as to minimize the data load and the number of operations performed at the L2GLB. The L2GLB is devoted to do the fine matching of the ECEM tower information with the FPS clusters.

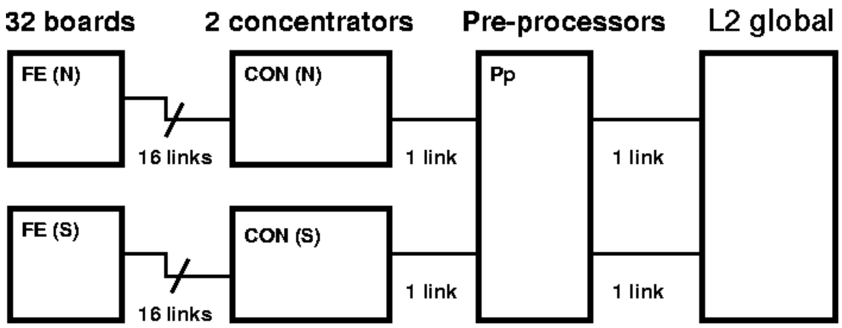

Figure 6.48: *Schematic of the L2 data path. All details on the links may be found in [6].*

The role of the L2PSpp is to translate the strip address from $(\mathrm{u},\mathrm{v}) \rightarrow (\eta,\phi)$ and then fill an array of dimension $(5,2)$ corresponding to the 0.2×0.2 EC trigger tower segmentation behind each FPS module. The (list of) object(s) must be treated within one module to simplify the operations. Thus, given the address of the lowest strip of the cluster and the cluster size, all the combinations between u and v strips have to be computed via a look-up table. Some of them are non-physical since they are out of the boundaries of the FPS module. They are rejected at this level. The physical combinations are sorted into $(\eta_{\mathrm{EC}},\phi_{\mathrm{EC}})$ bins defined from the ECEM trigger tower segmentation. The objects transferred from the FE boards to the L2Pp are detailed in the following section.

The role of the L2GLB is to count the coincidence of signals from an ECEM tower with the

FPS candidates in each of these bins. The objects transmitted from the L2PSpp to the L2GLB are defined in details in a next section.

6.3.2 L2 Objects transferred to from FE to L2PSpp

Table 12 reports the information we need to transmit to the L2PSpp. Beside the cluster orientation and type, the address and the width of the cluster are needed to perform the matching with the ECEM towers. The total count gives 32 bits. However, only 27 bits will be transferred, the rest of the 5 bits will be identified by the cable.

L2 Object (Pp)	Size in bit
Cluster orientation (U/V)	1 bit
Cluster type (ELE / GAM)	1 bit
Cluster address (low strip)	8 bits
Cluster width (max: 8)	3 bits
Upstream bit Mask	14 bits
TOTAL	27 bits
Info carried by CABLE	
Φ-sector (1 to 16) [cable]	4 bits
Side N/S [cable]	1 bit

Table 12: *Estimated bit counts per cluster sent from the FE boards to the L2Pre-processor.*

It should be noted that we decided to keep track of the bit mask in the upstream window (14-bits for a total of 7 strips) for physical motivations such as the triggering of isolated electrons as required for J/Ψ detection. This total of 32 bits matches well the constraint of the L2 structure, with 2 16-bits words per objects.

6.3.3 L2 Objects transferred to from L2Pp to L2GLB

Table 13 reports the information we need to transmit from L2PSpp to the L2GLB. Only the number of candidates per $(\eta_{\mathrm{EC}}, \phi_{\mathrm{EC}})$ bin are needed for the matching with ECEM tower signals.

L2 Object (GLB)	Size in bytes
η_{EC} bin (1 to 5) and cluster type (ELE,GAM)	1 byte
ϕ_{EC} bin (1 to 32)	1 byte
TOTAL	2 bytes

Table 13: *Estimated byte counts per cluster sent from the L2Pp to the L2GLB.*

All the L2 trigger will be described in details in an incoming dØnote [8].

A Summary of results

E/P_T in GeV	No EC threshold	EM tower threshold (EC)		
		$E_T \geq 2$ GeV	$E_T \geq 5$ GeV	$E_T \geq 10$ GeV
10 / 2.5	87.6±0.9%	86.5±2.3%	—	—
20 / 5.0	95.1±0.6%	96.6±0.8%	61.1±3.1%	—
40 /10.0	97.8±0.4%	98.9±0.4%	99.1±0.4%	100.0±0.0%
60 / 15.0	98.6±0.3%	99.3±0.4%	99.6±0.3%	99.7±0.3%
80 / 20.0	98.9±0.5%	99.4±0.6%	99.4±0.6%	99.1±0.6%
130/ 35.0	98.2±0.7%	98.9±0.8%	98.9±0.8%	98.9±0.8%

Table 1: Selection efficiency estimated on samples of single electron + 2mbias interactions. FPS Thresholds have been set at 0.3 MIPs upstream and 5 MIPs downstream. In column 2, only the FPS detector is used. In columns 2,3 and 4 efficiencies concern electrons already trigged by (at least) one EM tower in the EC quadrant with threshold of 2, 5 or 10 GeV in E_T.

E/P_T in GeV	No EC threshold	EM tower threshold (EC)		
		$E_T \geq 2$ GeV	$E_T \geq 5$ GeV	$E_T \geq 10$ GeV
10 / 2.5	23.7±1.5%	10.5±7.0%	—	—
20 / 5.0	26.9±1.6%	38.0±3.5%	—	—
40 / 5.0	31.8±1.6%	42.3±3.9%	49.9±5.8%	—
60 / 15.0	32.6±1.7%	44.8±2.8%	39.7±2.9%	30.6±6.3%
80 / 20.0	32.3±1.9%	46.1±4.5%	45.9±4.7%	50.0±6.2%
130/ 35.0	34.6±1.7%	45.7±2.8%	50.8±2.8%	51.9±3.0%

Table 2: Selection efficiency estimated on samples of single pions + 2mbias interactions. FPS Thresholds have been set at 0.3 MIPs upstream and 5 MIPs downstream. In column 2, only the FPS detector is used. In columns 2,3 and 4 efficiencies concern electrons already trigged by (at least) one EM tower in the EC quadrant with threshold of 2, 5 or 10 GeV in E_T.

E/P_T in GeV	No EC threshold	EM tower threshold (EC)	
		$T \geq 5$ GeV	$T \geq 10$ GeV
10 / 2.5	40.45±2.5%	09.55±1.5%	—
20 / 5.0	48.24±2.5%	42.71±2.5%	14.57±2.5%
40 /10.0	47.23±2.5%	48.24±2.5%	24.62±2.5%
60 / 15.0	50.00±2.5%	52.76±2.5%	28.39±2.5%
80 / 20.0	47.49±2.5%	48.74±2.5%	28.39±2.5%
130/ 35.0	54.77±2.5%	55.52±2.5%	33.16±2.5%

Table 3: Selection efficiency on single photon + 2mbias. Downstream threshold of 5MIPs and a VETO threshold of ≤0.3MIPs have been required in the FPS.

N(int)	Occupancy	
per crossing	MIP layer	Shower layer
1	3.71%	0.25%
2	6.08%	0.42%
3	8.45%	0.59%
4	10.82%	0.76%
5	13.19%	0.93%
6	15.56%	1.10%

Table 6: Occupancy as expected in the FPS detector for various number of interactions per crossing. The average number of extra interactions expected for $2\times10^{32}\mathrm{cm}^2.\mathrm{s}^{-1}$ and 99 bunch configuration is 2.

EM Threshold	$E_T \geq 2$ GeV	$E_T \geq 5$ GeV	$E_T \geq 10$ GeV
EC alone (1)	240,810 Hz	5,760 Hz	690 Hz
FPS + EC (2)	28,410 Hz	5,340 Hz	470 Hz
FPS + EC (3)	20,540 Hz	3,610 Hz	280 Hz
FPS + EC (4)	18,420 Hz	3,430 Hz	260 Hz

Table 7: Trigger rates for three combinations of FPS and EC information: a EM tower is required (1) to pass E_T threshold (2) to be confirmed by a FPS signal located on the same side (3) to be confirmed by a FPS signal located within the same quadrant (4) to be confirmed by a FPS signal located within the same octant. FPS thresholds have been set to 0.3 MIPs upstream and 5 MIPs downstream. Luminosity is $2 \times 10^{32} cm^2.s^{-1}$. Dijets are overlaid with 2 MinBias interactions.

Threshold in EC	$E_T \geq 2$ GeV	$E_T \geq 5$ GeV	$E_T \geq 10$ GeV
EC alone	240,810 Hz	5,760 Hz	690 Hz
EC + FPS (T=5 MIPs)	20,540 Hz	3,610 Hz	280 Hz
EC + FPS (T=10 MIPs)	9,120 Hz	1,920 Hz	160 Hz

Table 8: Electron trigger rates computed on di-jets + 2 MinBias interactions events using the EC calorimeter alone (1^{st} row) or combining the FPS and EC trigger tower within the same quadrant (2^{nd} and 3^{rd} rows). FPS thresholds have been set to 0.3 MIPs upstream and 5 or 10 MIPs downstream. Luminosity is $2 \times 10^{32} cm^2.s^{-1}$

Threshold in EC	$E_T \geq 2$ GeV	$E_T \geq 5$ GeV	$E_T \geq 10$ GeV
EC alone	240,810 Hz	5,760 Hz	690 Hz
EC + FPS (T=5 MIPs)	28,140 Hz	4,830 Hz	490 Hz
EC + FPS (T=10 MIPs)	14,310 Hz	2,840 Hz	240 Hz

Table 9: EM trigger rates computed on di-jets + 2 MinBias events using the EC calorimeter alone (1^{st} row) or combining the FPS and EC trigger tower within the same quadrant (2^{nd} and 3^{rd} rows).FPS thresholds have been set to 0.3 MIPs upstream and 5 or 10 MIPs downstream. Luminosity is $2 \times 10^{32} cm^2.s^{-1}$

Threshold in EC	$E_T \geq 2$ GeV	$E_T \geq 3$ GeV	$E_T \geq 4$ GeV	$E_T \geq 5$ GeV
EC alone	34,600 Hz	15,280 Hz	9,020 Hz	4,580 Hz
EC + FPS (T=5 MIPs)	5,900 Hz	4,440 Hz	4,400 Hz	2,520 Hz
EC + FPS (T=10 MIPs)	820 Hz	580 Hz	520 Hz	240 Hz

Table 10: Di-Electron trigger rates computed on di-jets events using the EC calorimeter alone (1^{st} row) or combining the FPS and EC trigger tower within the same quadrant (2^{nd} and 3^{rd} rows). FPS thresholds are set to 0.3 MIPs upstream and 5 MIPs or 10 MIPs downstream. Luminosity is $\mathcal{L} = 2 \times 10^{32} \mathrm{cm}^2.\mathrm{s}^{-1}$. All samples have been overlaid with 2 minbias interactiions.

L1 object (TM)	Size in bit(s)
Cluster orientation (U/V)	1 bit
Cluster type (ELE / GAM)	1 bit
TOTAL	2 bits
Info carried by CABLE	
Φ-sector (1 to 4) [cable]	2 bits
Side N/S [cable]	1 bit

Table 11: Object treated at the L1 Trigger Manager and size in bits. Each object sent from each FE to the TM has a 2-bits size, while the Phi-sector as well as the side of the cluster are identified by the cable. See the text for the role of the concentrator.

L2 Object (Pp)	Size in bit
Cluster orientation (U/V)	1 bit
Cluster type (ELE / GAM)	1 bit
Cluster address (low strip)	8 bits
Cluster width (max: 8)	3 bits
Upstream bit Mask	14 bits
TOTAL	27 bits
Info carried by CABLE	
Φ-sector (1 to 16) [cable]	4 bits
Side N/S [cable]	1 bit

Table 12: Estimated bit counts per cluster sent from the FE boards to the L2Pre-processor.

References

[1] The DØupgrade for the FPS, Muon and L2 trigger, FERMILAB-FN-641, DØnote 2894.

[2] "NFS Proposal for a Muon Level-2 Preprocessor dor DØ" by Mike Fortner, DØcollaboration

[3] "TDR of the Forward Preshower detector for the d0 upgrade" J. Kotchaer et al.

[4] Trigger for CPS and FPS.xxxx in preparation xxx

[5] "Results from a Beam test of the FPS detector for the DØupgrade", Arnaud Lucotte and Mrinmoy Bhattacharjee, DØ-note/3398.

[6] WEB server: http://d0server1.fnal.gov/users/borcherding/Fred_home.html.

[7] WEB server: http://www-d0.fnal.gov/ klopfens/lum20.html

[8] "The L2 trigger using the FPS detector" M. Bhattacharjee and A. Lucotte, in preparation.